AGU PUBLICATIONS

JGR

Journal of Geophysical Research: Atmospheres

RESEARCH ARTICLE
10.1002/2017JD026504

Key Points:
- NOAA NUCAPS and coincident UCAR COSMIC GPS RO dry temperature profiles are compared to Vaisala RS92 radiosondes
- NUCAPS bias relative to radiosondes from 40 to 100 hPa is under 0.5 K with RMS error under 1 K when temperature averaging kernels are applied
- NOAA NUCAPS agreement with NASA AIRS and EUMETSAT IASI is less than 0.5 K using COSMIC RO as a common reference

Supporting Information:
- Supporting Information S1
- Figure S1
- Figure S2
- Figure S3
- Figure S4
- Figure S5
- Figure S6

Correspondence to:
M. L. Feltz,
michelle.feltz@ssec.wisc.edu

Citation:
Feltz, M. L., L. Borg, R. O. Knuteson, D. Tobin, H. Revercomb, and A. Gambacorta (2017), Assessment of NOAA NUCAPS upper air temperature profiles using COSMIC GPS radio occultation and ARM radiosondes, *J. Geophys. Res. Atmos.*, *122*, 9130–9153, doi:10.1002/2017JD026504.

Received 17 JAN 2017
Accepted 1 AUG 2017
Accepted article online 7 AUG 2017
Published online 7 SEP 2017

Assessment of NOAA NUCAPS upper air temperature profiles using COSMIC GPS radio occultation and ARM radiosondes

M. L. Feltz[1], L. Borg[1], R. O. Knuteson[1], D. Tobin[1], H. Revercomb[1], and A. Gambacorta[2]

[1]Space Science and Engineering Center, University of Wisconsin-Madison, Madison, Wisconsin, USA, [2]Science and Technology Corporation, Hampton, Virginia, USA

Abstract The U.S. National Oceanic and Atmospheric Administration (NOAA) recently began operational processing to derive vertical temperature profiles from two new sensors, Cross-Track Infrared Sounder and Advanced Technology Microwave Sounder, which were developed for the next generation of U.S. weather satellites. The NOAA-Unique Combined Atmospheric Processing System (NUCAPS) has been developed by NOAA to routinely process data from future Joint Polar Satellite System operational satellites and the preparatory Suomi-NPP satellite. This paper assesses the NUCAPS vertical temperature profile product from the upper troposphere into the middle stratosphere using radiosonde and GPS radio occultation (RO) data. Radiosonde data from the Department of Energy Atmospheric Radiation Measurement (ARM) program are=] compared to both the NUCAPS and GPS RO temperature products to evaluate bias and RMS errors. At all three fixed ARM sites for time periods investigated the NUCAPS temperature in the 100–40 hPa range is found to have an average bias to the radiosondes of less than 0.45 K and an RMS error of less than 1 K when temperature averaging kernels are applied. At a 95% confidence level, the radiosondes and RO were found to agree within 0.4 K at the North Slope of Alaska site and within 0.83 K at Southern Great Plains and Tropical Western Pacific. The GPS RO-derived dry temperatures, obtained from the University Corporation for Atmospheric Research Constellation Observing System for Meteorology, Ionosphere, and Climate (COSMIC) mission, are used as a common reference for the intercomparison of NUCAPS temperature products to similar products produced by NASA from Atmospheric Infrared Sounder (AIRS) and by European Organisation for the Exploitation of Meteorological Satellites from MetOp-B Infrared Atmospheric Sounding Interferometer (IASI). For seasonal and zonal scales, the NUCAPS agreement with AIRS and IASI is less than 0.5 K after application of averaging kernels.

1. Introduction

The U.S. National Oceanic and Atmospheric Administration (NOAA) recently began operational processing to derive vertical temperature profiles from the Advanced Technology Microwave Sounder (ATMS) and the Cross-Track Infrared Sounder (CrIS) instruments housed on board the Suomi-NPP satellite. Suomi-NPP was launched in 2011 by the National Aeronautics and Space Administration (NASA) into the same PM Sun-synchronous orbit as the Earth Observing System (EOS) Aqua platform in preparation for the transition to the operational Joint Polar Satellite System (JPSS) satellite series, which is planned to provide global daily coverage in the traditional PM Sun-synchronous orbit beginning in 2017 [*Murphy*, 2006; *Gleason et al.*, 2012; *Goldberg et al.*, 2013]. The NOAA-Unique Combined Atmospheric Processing System (NUCAPS) was developed by NOAA to routinely process data from future JPSS operational weather satellites [*Gambacorta et al.*, 2012]. The ground processing software uses observations from both the ATMS and CrIS instruments—two of the sensors developed for the JPSS satellite series [*Weng et al.*, 2012; *Han et al.*, 2013]. The NUCAPS software replaces a vendor-supplied algorithm known as the Cross-track Infrared Microwave Sounding Suite (CrIMSS) Environmental Data Record (EDR) [*Divakarla et al.*, 2014]. The Suomi-NPP products are available from NOAA's Comprehensive Large Array-data Stewardship System (CLASS). A version of the NUCAPS software is also publicly available for use with either archived data or from the Suomi-NPP direct broadcast signal.

This paper presents an assessment of the NUCAPS atmospheric vertical temperature profile product from the upper troposphere into the lower to middle stratosphere, an otherwise difficult region to perform such assessments due to the challenge of obtaining reliable ground truth at these altitudes. The assessment uses in situ radiosonde upper air observations from the Department of Energy (DOE) Atmospheric Radiation Measurement (ARM) program at sites on the North Slope of Alaska (NSA-Barrow), Southern Great Plains

(SGP-Lamont), and Tropical Western Pacific (TWP-Darwin) [*Stokes and Schwartz*, 1994]. In addition, these data are complemented uniquely with Global Positioning System (GPS) radio occultation (RO)-derived dry temperature profiles from the University Corporation for Atmospheric Research (UCAR) Constellation Observing System for Meteorology, Ionosphere, and Climate (COSMIC) mission [*Kursinski et al.*, 1997; *Hajj et al.*, 2002; *Schreiner et al.*, 2007; *Anthes et al.*, 2008; *Ho et al.*, 2014]. A recent study by *Nalli et al.* [2017] also makes an assessment of NUCAPS temperature and moisture products using radiosonde, ocean campaign data, and model data.

Traditionally, radiosondes have been used to provide an absolute reference for the evaluation of microwave (MW) and infrared (IR) sounding products [*Fetzer et al.*, 2003; *Tobin et al.*, 2006; *Divakarla et al.*, 2006, 2009; *Nalli et al.*, 2013; *Sun et al.*, 2010, 2013]. The era of near-real-time soundings from high spectral resolution infrared sounders began with the EOS Atmospheric Infrared Sounder (AIRS) launched in 2002 on the NASA Aqua platform [*Goldberg et al.*, 2003]. The need for an improved validation methodology for evaluating AIRS retrieval products lead to the use of the DOE ARM sites for dedicated launches of research quality radiosondes. Launches of radiosondes were timed prior to Aqua satellite overpasses to minimize atmospheric state uncertainties [*Tobin et al.*, 2006]. In this study, atmospheric state uncertainties are minimized by making use of operational ARM radiosonde data which are spatiotemporally coincident to Suomi-NPP CrIS NUCAPS retrievals. While dedicated ARM upper air in situ measurements were performed in coordination with the Global Climate Observing System Reference Upper-Air Network (GRUAN) program at the ARM sites [*Bodeker et al.*, 2016], they are not used in this study.

The COSMIC RO data are used in this study as a common reference for the intercomparison of Suomi-NPP NUCAPS temperature profile products with similar retrieval products routinely produced from hyperspectral infrared and microwave sounders on board NASA's EOS Aqua and European Organisation for the Exploitation of Meteorological Satellites' (EUMETSAT) MetOp satellites—specifically the NASA AIRS Science Team version 6 (ASTv6) and the official EUMETSAT Infrared Atmospheric Sounding Interferometer (IASI) (EUMv6) retrieval. Though NOAA offers an IASI retrieval product, this study focuses on the IR sounder operational products offered by their associated institutions—additionally, a comparison of NOAA IASI with UCAR RO products was made in previous studies [*M. Feltz et al.*, 2014]. To facilitate the comparison of these three independent IR retrievals using RO as a reference, averaging kernels (AKs) are computed using a consistent methodology for each AIRS, IASI, and CrIS retrieval that is found to be spatiotemporally coincident with a RO profile or radiosonde. An infrared radiative transfer model (RTM) is employed for this purpose to compute temperature Jacobians, which are needed for the AK computation. The AKs, which are used to smooth the higher vertical resolution RO profiles, are calculated specifically for the 15 μm, carbon dioxide absorption region channels. Thus, the AKs represent the theoretical resolution of the IR sounder and are used to smooth the IR retrievals using a uniform method—they do not represent the exact retrieval AKs which are based off of both MW and IR information and correspond to a different set of channels. The choice of IR only AKs is chosen to provide a lowest common denominator for the information content for the sole purpose of making a comparison with the RO. Any possible information in the IR/MW retrievals which has higher vertical structure, whether from MW or from regression/neural net to numerical weather prediction profiles, etc., will be filtered out by the IR-only AKs for the purpose of this comparison.

A focus is given to the upper troposphere to middle stratosphere region between ~40 and 100 hPa where RO temperatures have been shown to have the highest accuracy and are best suited to act as a common reference [e.g., *Das and Pan*, 2014; *Alexander et al.*, 2014; *Steiner et al.*, 2013; *Foelsche et al.*, 2011; *Scherllin-Pirscher et al.*, 2011a; *Schreiner et al.*, 2007]. For this work, the RO dry temperature product is used, which derives temperature from a refractivity profile assuming that there is no water vapor. The COSMIC dry temperature product was successfully used to evaluate temperature retrievals from the CrIMSS EDR product in the desired pressure range by *M. Feltz et al.* [2014].

Section 2 of this paper provides background on GPS RO, section 3 describes data used in this study, section 4 discusses methodology, and sections 5 and 6 give results for ARM site and global, zonal comparisons, respectively. An appendix is included which provides detail on the calculation and application of averaging kernels which are used in this analysis. Intermediate results prior to the application of averaging kernels are included as supporting information.

2. GPS RO Background

GPS RO is valuable when used as a common reference for IR/MW sounding product assessment because it uses an independent measuring technique, provides thousands of globally distributed vertical temperature profiles per day (assuming that an adequate constellation of receivers such as the COSMIC network is available), and provides a measurement whose spatial resolution is one that the MW/IR sounder profiles can be matched to, unlike exact point profiles as provided by radiosondes. Additionally, RO performs well in the tropopause region where thermal sounders have lower information content due to the isothermal nature of the atmosphere. Typically, the vertical resolution of the RO observations ranges from 0.5 km in the lower troposphere to 1.4 km in the middle atmosphere [*Kursinski et al.*, 1997]. *Wee and Kuo* [2015] recently made use of the high-quality RO-measured phase paths and successfully used them to assess model forecasts and reanalyses.

To derive RO dry temperature, bending angles and refractivity are calculated as intermediate products in the processing of phase delay measurements. From refractivity, dry temperature is calculated assuming no water vapor, which is an acceptable assumption for altitudes above the upper troposphere. However, assumptions about ionospheric contributions to refractivity are also made and seem to be the most challenging to account for. While zeroth-order contributions are removed from RO profiles at higher altitudes, residual errors can be amplified by the processing scheme and propagate downward in altitude to affect the dry temperature down to ~35 hPa [*Syndergaard*, 2000; *Mannucci et al.*, 2006, 2011; *Danzer et al.*, 2013]. Though prone to such residual ionospheric errors, RO dry temperatures do not intake any numerical weather prediction model as background and thus are not contaminated by potential weather model biases. Errors and uncertainties of the RO-derived temperatures have been studied by different groups using various methods. Examples, which are not exhaustive, include comparisons of versions from different processing centers [*Gorbunov et al.*, 2011; *Ho et al.*, 2012], comparisons of RO to other instruments or model analyses [e.g., *Das and Pan*, 2014; *Ladstädter et al.*, 2014, 2011; *Kuo et al.*, 2005], studies of ionospheric influences [e.g., *Liu et al.*, 2015; *Verkhoglyadova et al.*, 2015; *Danzer et al.*, 2013; *Mannucci et al.*, 2011], assessing RO data's utility in providing climate records [e.g., *Foelsche et al.*, 2011b; *Steiner et al.*, 2013, 2011], or mixes of all these and others [e.g., *Gorbunov and Kirchengast*, 2015; *Foelsche et al.*, 2011a; *Scherllin-Pirscher et al.*, 2011a, 2011b]. The use of RO-derived temperatures in the upper troposphere, lower stratosphere as an absolute reference has grown in recent years, as it has been used to identify radiosonde biases [*He et al.*, 2009; *Sun et al.*, 2013], evaluate model reanalyses [e.g., *Kishore et al.*, 2016], and calibrate MW sounders [e.g., *Ho et al.*, 2009; *Zou et al.*, 2014; *Isoz et al.*, 2015], in addition to evaluating hyperspectral IR sounder temperatures [*Yunck et al.*, 2009; *M. Feltz et al.*, 2014]. Comparisons of COSMIC temperatures to Atmospheric Chemistry Experiment-Fourier Transform Spectrometer v3.5 showed agreement up to 1 K for altitudes between 15 and 40 km (~100–3 hPa) [*Olsen et al.*, 2016], while comparisons to Sounding of the Atmosphere using Broadband Emission Radiometry and Microwave Limb Sounder showed agreement over all seasons from 80°N–80°S and 100–10 hPa being under 3 and 2 K, respectively [*Das and Pan*, 2014]. Much headway has been attained in recent literature in regard to identifying improvements upon the RO measuring system—in both instrument technology and the processing techniques [e.g., *Wang et al.*, 2016; *Li et al.*, 2015; *Zeng et al.*, 2015]. Though RO products have been proven to be of considerable value, scant literature exists that assigns an absolute uncertainty to the derived dry temperature products as a function of altitude. For this reason, the current study uses RO profiles primarily as a stable common reference for comparison of NUCAPS products with similar products from other IR sounders and not as an absolute reference. While any RO mission could be used to provide stable dry temperature products, the COSMIC network was chosen for this study since it is able to provide ample matchup cases for CrIS, IASI, and AIRS. Derived RO dry temperature profiles are known to be of highest quality within the upper troposphere to lower stratosphere (UTLS) (40–100 hPa) region where focus is set for this study.

3. Data

3.1. Thermal Sounders

NUCAPS temperature products, which are derived from measurements of the CrIS and ATMS instruments, are available operationally from the NOAA CLASS (see https://www.class.noaa.gov). The archival dataset in CLASS consists of a time record composed of several important version updates of the NUCAPS software as well as different versions of the CrIS radiance record; however, the data used for this study are derived from a

Table 1. IASI, AIRS, and CrIS Instrument and Currently Operational Retrieval Characteristics

	IASI	AIRS	CrIS (Normal Spectral Resolution)
		Instrument Differences	
Spectral coverage and range	No gaps 645–2760 cm^{-1}	17 bands, with gaps 645—2674 cm^{-1}	three bands, with gaps 645–1095 cm^{-1} 1210–1750 cm^{-1} 2155–2550 cm^{-1}
Spectral sampling	0.5 cm^{-1}	0.4–2.1 cm^{-1} (varies by band)	LWIR: 0.625 cm^{-1} MWIR: 1.25 cm^{-1} SWIR: 2.5 cm^{-1}
Size of field of view (nadir)	12 km	13.5 km	14 km
Type	Fourier transform IR spectrometer	Grating spectrometer	Fourier transform IR spectrometer
Platform	Metop-B	Aqua	Suomi-NPP
Local equator crossing times	9:30	13:30	13:30
Spatial coverage	2 × 2 FOV in ~50 km^2	3 × 3 FOV in ~50 km^2	3 × 3 FOV in ~50 km^2
Swath width	2200 km	1650 km	2200 km
		Algorithm Differences	
Retrieval type	EUMETSAT v6 PWLR_MWIR: Statistical regression retrieval using air mass classification	AIRS Science Team v6: Physical retrieval with first guess defined by the previously retrieved, cloud cleared MW retrieval	NUCAPS: Physical retrieval with first guess defined by the previously retrieved, cloud cleared MW retrieval
# FOVs/retrieval	1	9	9
Cloud clearing	no	yes	yes

consistent reprocessing of the CrIS radiance record using software publicly available from the Community Satellite Processing Package (CSPP) (see http://cimss.ssec.wisc.edu/cspp/). The radiance record uses CSPP SDR v2.1, and the NUCAPS retrieval uses CSPP NUCAPS v1.0.

The NUCAPS EDR files are used to obtain temperature and pressure profiles at 101 vertical levels and the variable "View_Angle." Only profiles with a "Quality Flag" variable of accepted are used.

Temperature profile products derived from NASA's Atmospheric Infrared Sounder (AIRS)/Advanced Microwave Sounding Unit (AMSU), instruments on board the Aqua satellite, are obtained from the Goddard Earth Sciences Data and Information Services Center (see http://disc.sci.gsfc.nasa.gov). The Level 2 version 6.0 Support Product is used, which provides temperature measurements at 101 vertical pressure levels [*Susskind et al.*, 2011]. Quality control on this product consists of using the AIRS L2 "Pbest" quality flag, which determines how deep into the atmosphere the satellite retrieval is considered to be valid [*Susskind et al.*, 2011]. Level 1 version 5 AIRIBRAD radiance files are also used for obtaining instrument scan angles.

The Infrared Atmospheric Sounding Interferometer (IASI) instrument [*Blumstein et al.*, 2004] is flying on board Metop satellites as part of the EUMETSAT Polar System program [*Klaes et al.*, 2007]. In order to use a most recent version of the Level 2 products [*August et al.*, 2012] consistently with the other data sets, the atmospheric temperatures were provided directly by EUMETSAT. They are generated with a statistical retrieval method called the Piece-Wise Linear Regression (PWLR), which forms the first guess all-sky products of the version 6.0 processor activated on 30 September 2014 and disseminated in near-real time since. The PWLR uses European Centre for Medium-Range Weather Forecasts (ECMWF) analyses model fields for training and exploits MW (AMSU + Microwave Humidity Sounder) and IR (IASI) measurements jointly as sole inputs for retrievals. These products were assessed in a study by *Roman et al.* [2016]. Specifically, data are used from the IASI on board the Meteorological Operational satellite-B. Only profiles whose "FLG_BAD" variable is not equal to 0 are used. Corresponding instrument scan angles were estimated using knowledge of IASI's field of view geometry.

The term "IR sounder" is hereafter used in this paper to represent the combined use of both microwave (MW) and infrared (IR) sounding channels. This distinguishes the combined product from an MW-only product such as is produced by the NOAA Microwave Integrated Retrieval System algorithm [*Boukabara et al.*, 2011]. Table 1 lists basic characteristics of the CrIS, AIRS, and IASI instruments and the retrievals used in this study. Differences seen between the three sounders in characteristics such as those listed in the table are potential contributors to the differences seen in the retrieval performances with respect to the COSMIC common reference.

3.2. Radiosondes

ARM Climate Research Facility data were retrieved through the Department of Energy ARM data archive (http://www.archive.arm.gov/arm). The Vaisala RS92 processed radiosonde temperatures were used from the Tropical Western Pacific Darwin (TWP), Northern Slope of Alaska Barrow (NSA), and Southern Great Plains Lamont, Oklahoma (SGP) sites. Only good profiles indicated by "qc_tdry" and "qc_pres" variables being equal to 0 are used. The Vaisala RS92 has a stated uncertainty of 0.5 C from 60 to −90 C with a resolution of 0.1 C, a repeatability of 0.15 C, and a reproducibility of 0.2 C (1080–100 hPa), 0.3 C (100–20 hPa), and 0.5 C (20–3 hPa) (Vaisala Radiosonde RS92 Datasheet, http://www.vaisala.com/Vaisala%20Documents/Brochures%20and%20Datasheets/RS92SGP-Datasheet-B210358EN-F-LOW.pdf).

3.3. Radio Occultation

The U.S./Taiwanese COSMIC, or Taiwan's Formosa Satellite Mission #3 (FORMOSAT-3), is a mission consisting of six radio receivers on low Earth orbiting satellites in circular 72° inclination orbits and has been ongoing since April 2006 [*Anthes et al*., 2008]. Originally, the COSMIC network produced around 2000 profiles per day; however, loss of contact to various satellites has caused the number of profiles to decrease over time. Data are obtained from the UCAR COSMIC Data Analysis and Archive Center (http://cdaac-www.cosmic.ucar.edu/). The climate-processed "cosmic2013" dry temperature product (version 2013.3520) is used and is referred to here as either "COSMIC" or "COSMIC2013." Applied quality control consists of excluding profiles marked "bad."

3.4. Radiative Transfer Model and Input

The RTM employed in this study for the AK computation is the Optimal Spectral Sampling (OSS) fast model [*Moncet et al*., 2008, 2015]. OSS does computations on 101 fixed pressure levels that range from 1100 to 0.005 hPa. More details of the calculations are given in the appendix, and following statements describe data used for input into the RTM.

Carbon dioxide (CO_2) data are obtained from CarbonTracker (CT), NOAA's Earth System Research Laboratory CO_2 measurement and modeling system. Version CT2013, available for 2000–2012 as global 3° × 2° gridded monthly CO_2 mole fractions, is used (http://carbontracker.noaa.gov).

Ozone, skin temperature, water vapor, and surface pressure are obtained from ECMWF's ERA-Interim reanalysis model which is run on 6-hourly increments (http://www.ecmwf.int/en/research/climate-reanalysis/era-interim) [*Dee et al*., 2011]. The 0.75° gridded model level product has resolution equivalent to ~80 km and is available up to ~0.1 hPa.

4. Methods

The approach chosen for this study is to find the global time and space coincident profiles for the IR sounder and the COSMIC RO dry temperature profiles within the time period of interest, which is 3 years from April 2012 to May 2015 (except for IASI which is 1 year from April 2013 to May 2014). This paper uses the raypath method described in *M. L. Feltz et al*. [2014], which minimizes spatiotemporal mismatch error by using a 1 h time criterion between IR and RO profiles and by creating an average IR profile from the 101 retrieved IR sounder levels. This "raypath-averaged" profile captures the variation of RO latitude and longitude with height and the unique RO horizontal resolution (about 270 km) along the occultation raypath. This method was previously used in *M. Feltz et al*. [2014] to compare temperature profiles derived from CrIS, AIRS, and IASI for a limited time period on 30° global latitude zones. This paper applies the same method to a longer time series of data and targets the current operational satellite profile products distributed by the satellite agencies NOAA, NASA, and EUMETSAT.

A subset of the IR and RO matchups was found that are within 3 h and 300 km of a radiosonde launch from one of the three ARM sites—NSA, SGP, or TWP. This leads to a much smaller data set where IR, RO, and radiosonde profiles exist in coincidence for each ARM site. For this restricted matchup subset, the profile differences taken as IR minus radiosonde, IR minus RO, and RO minus radiosonde are each analyzed in terms of bias and root-mean-square (RMS) error. Note that in this matchup set, the IR and RO profiles are spatially coincident with a 270 km horizontal averaging scale, while the Vaisala radiosonde is an in situ point measurement which can be offset in latitude/longitude by up to 300 km. Figure 1 illustrates a NUCAPS matchup example

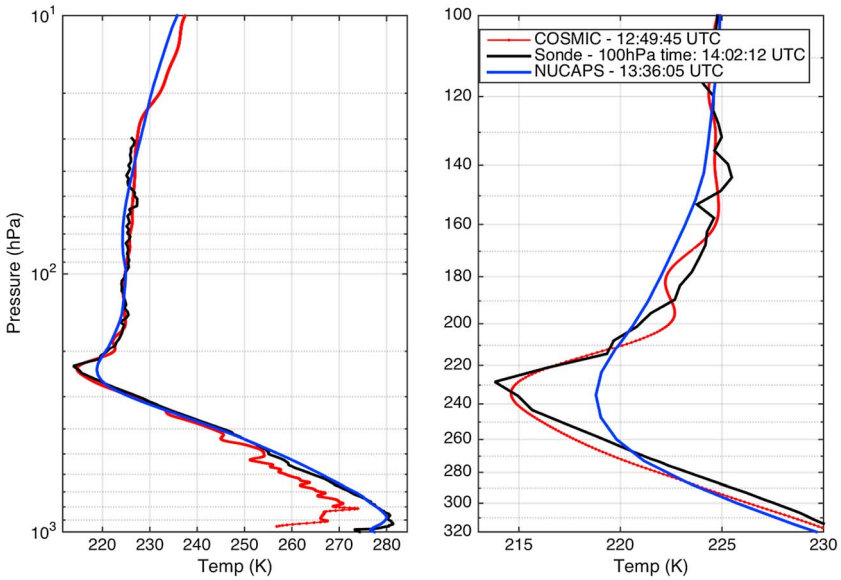

Figure 1. Overlay of NSA ARM radiosonde (black), COSMIC (red), and NUCAPS (blue) temperature profiles for (left) 14 August 2014 with a (right) zoomed view of the tropopause.

from the ARM NSA site on 14 August 2014 at about 13:36 UTC and exemplifies the higher vertical resolution of the radiosonde and RO temperature profiles. The zoomed view around the tropopause region shows that the IR sounder is not able to resolve the cold tropopause layer as is the RO and radiosonde, which is expected due to the IR sounders more limited vertical resolving capability. While this represents an error of the IR profile relative to the true atmosphere, a quantitative assessment of the NUCAPS algorithm against a truth data set with higher vertical resolution benefits from a smoothing of the higher vertical resolution observations to match the lower resolution IR sounding.

To account for the IR vertical resolution, two different approaches to vertical averaging are applied to the IR sounder minus RO differences. The first analysis approach, used in previous IR sounder validation studies, applies an approximately 1 km slab layering to the difference profiles [*Susskind et al.*, 2003; *Divakarla et al.*, 2006; *Tobin et al.*, 2006; *Nalli et al.*, 2013; *M. L. Feltz et al.*, 2014; *M. Feltz et al.*, 2014; *Nalli et al.*, 2017]. A table in *M. Feltz et al.* [2014] provides the layer thicknesses (1 to 3 km) of the slab layering method in the vertical range of interest. The second analysis approach is to compute IR sounder vertical averaging kernels (AKs) for temperature profiles appropriate for each matchup case and then to apply them to the vertical temperature profile differences. Since the RO and radiosonde have higher vertical resolution, no RO or radiosonde AK is needed. The averaging kernels are used to smooth profile differences between IR and RO products or NUCAPS and ARM radiosondes. This smoothing reduces the higher vertical resolution of the RO and radiosonde profiles to match that of the IR sounder [*Rodgers and Connor*, 2003]. Simultaneous application of the same averaging kernel to the IR sounder profile also removes vertical oscillations within the null space of the infrared retrievals [*Rodgers*, 1990]. Appendix A1 details the method of calculating and applying the averaging kernels, further discusses the different averaging techniques, and includes a forward calculation perturbation study on the importance of including proper sensor view angles in the averaging kernel calculation.

To summarize the analysis results, the average bias, average uncertainty in the mean, and average RMS are computed over the atmospheric pressure range of 40 to 100 hPa for the ARM site comparisons. This range is chosen to be above the regions where possible contamination of the RO dry temperature profile can occur due to significant amounts of atmospheric water vapor and to be below the region where the balloons used to carry ARM radiosondes aloft tend to burst. This same 40 hPa to 100 hPa altitude range is used to characterize the global zonal IR sounder minus COSMIC RO results in order to facilitate comparison with the ARM site results and also to avoid regions where RO ionospheric errors grow with increasing altitude above ~35 hPa. A separate average is computed for the 15 hPa to 40 hPa altitude range for the global zonal COSMIC RO comparison to gain insight into the IR/RO comparison in the middle stratosphere region.

Table 2. ARM Site Radiosonde, COSMIC, and NUCAPS Matchup Statistics Averaged Over the 40 to 100 hPa Vertical Range for the 3 Year Time Period April 2012 Through May 2015[a]

ARM Radiosonde, COSMIC, and NUCAPS Matchup Statistics 40–100 hPa Average									
	AK*(NUCAPS-Ro)			AK*(NUCAPS-Sonde)			RO-Sonde		
	Bias	2*Unc.	RMS	Bias	2*Unc.	RMS	Bias	2*Unc.	RMS
NSA annual	−0.144	0.151	1.10	−0.203	0.0926	0.70	−0.130	0.258	1.78
SGP summer	−0.291	0.199	0.796	−0.089	0.176	0.66	0.229	0.576	2.00
SGP winter	−0.174	0.155	0.526	−0.145	0.293	0.95	−0.008	0.649	2.02
TWP annual	−0.174	0.189	0.405	−0.171	0.176	0.371	−0.068	0. 764	1.41

[a]Uncertainties are 2 times the uncertainty of the mean ($k = 2$). Collocation criteria require the matchups to occur less than 300 km away from the ARM site and that the time of the radiosonde is within 3 h of the RO and NUCAPS matchup time (see text for details).

Results for altitudes above 15 hPa are not presented due to increasing uncertainty in the RO-derived product profiles [*Steiner et al.*, 2013].

5. NUCAPS, COSMIC, and ARM Site Radiosonde Comparisons

Results are shown in Table 2 for average bias and RMS errors in the 40 to 100 hPa vertical range for the NSA, SGP, and TWP site NUCAPS, radiosonde, and COSMIC RO matchups. The NUCAPS averaging kernels are applied to the NUCAPS-RO and NUCAPS-sonde difference profiles but not to the RO-sonde differences. The column label 2*Unc represents 2 times the 1σ uncertainty in the mean, i.e., 2*Unc = $2*\sigma/\mathrm{sqrt}(N)$ where σ is the standard deviation and N is the number of profiles in the sample set. Since it can be assumed that the matchup samples are independent, 2*Unc is the 95% confidence interval of the bias estimate. Overall, in the 40 hPa to 100 hPa altitude range, the NUCAPS minus radiosonde bias with uncertainty of less than ~0.44 K magnitude (seen as a maximum in SGP winter) is well within the stated 0.5 K uncertainty of the Vaisala RS92 radiosondes at each of the ARM sites. Because no averaging kernel is used in the RO to sonde comparisons, the fact that sondes represent point measurements while RO profiles represent larger volumes of atmosphere contributes to the difference statistics. This difference in measurement techniques is likely one of the reasons that the RMS statistics for the RO minus sonde differences are largest across all sites/seasons.

5.1. North Slope of Alaska ARM Site

Figure 2 (top row) shows 3 years of bias and RMS statistics between COSMIC, NUCAPS, and ARM radiosondes over the ARM NSA site. The panel labeled "# Samples" shows the number of samples at each of the retrieval levels. NUCAPS and RO have 209 samples at all heights, but the height of the balloon burst leads to a decrease in the number of radiosonde temperature samples with height. Also shown in this panel is the sum of the averaging kernel rows times 100. The closer the value is to 100, the larger percentage of information that is coming from the truth profile and the less from the a priori state [*Rodgers*, 1976]. The column labeled "101 level" are comparisons at the original NUCAPS retrieval levels without vertical smoothing. The "1 km layer" column has 1 km slab layering applied. The "AK Applied" column shows results where averaging kernels are applied to the individual difference profiles prior to computing the bias and RMS statistics. The dotted lines on either side of the solid lines show the 2σ uncertainty in the estimate of the mean bias.

Within the calculated uncertainties at the NSA site, COSMIC shows excellent agreement with the ARM radiosondes from 20 hPa to 200 hPa in both the 101 level and ~1 km slab layer result. NUCAPS biases relative to both the radiosonde and COSMIC, however, lie outside of the 2σ uncertainty range for the 101 level and ~1 km layer result. In particular, the NUCAPS biases contain a negative to positive vertical oscillation over the 200 to 50 hPa range. After application of the CrIS averaging kernels, this vertical oscillation of the biases is removed, and NUCAPS is seen to agree quite well with both the radiosonde and COSMIC RO profiles. Specifically, NUCAPS appears to be in excellent agreement with the radiosondes over the 200–10 hPa vertical range and has an RMS value that is decreased within the 100–40 hPa range from ~1.2 K in the 101 level results to ~0.6 K after AK application. It should be noted that the NUCAPS minus radiosonde bias is slightly negative by ~0.2 K between ~160 and 80 hPa. Meanwhile, the NUCAPS bias agrees with COSMIC after AK application from ~55 to 200 hPa, and the RMS is similarly decreased, though it is still larger than the NUCAPS minus radiosonde RMS. The disagreement of COSMIC and NUCAPS at these higher altitudes of above ~35 hPa is likely

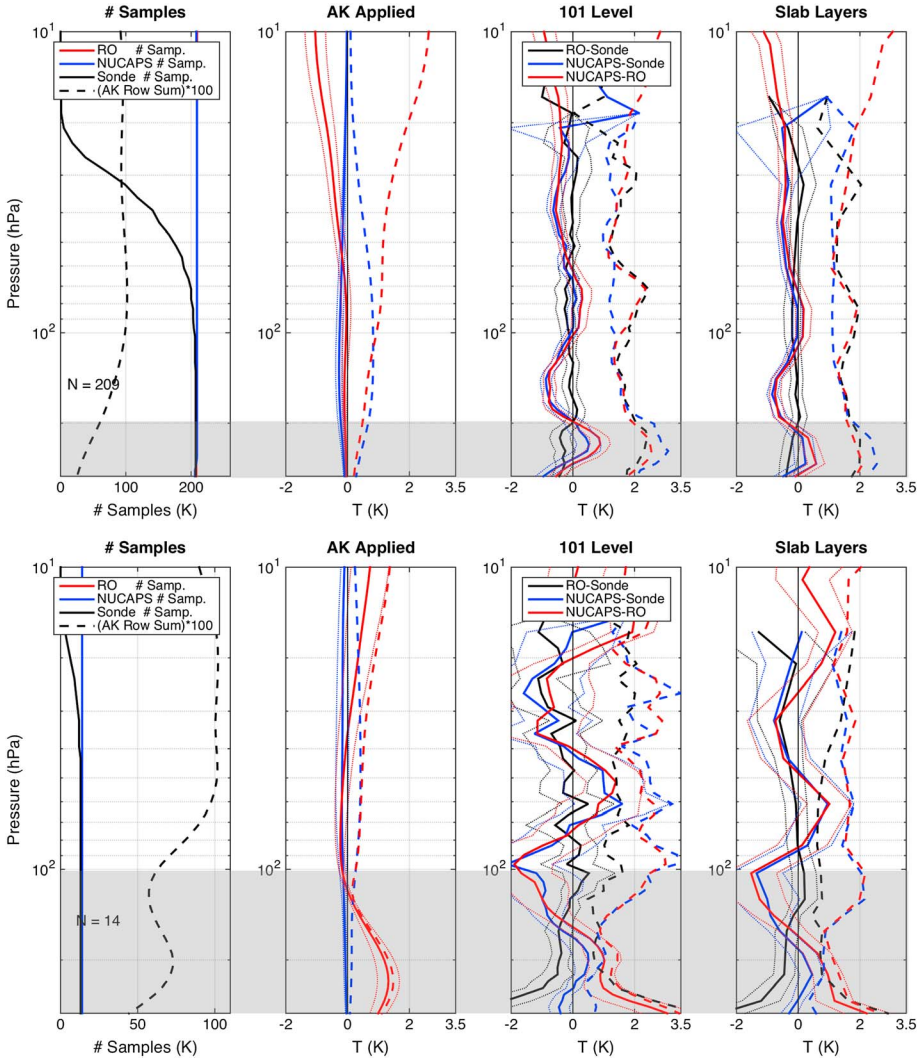

Figure 2. ARM radiosonde, COSMIC, and NUCAPS matchup statistics. Statistics of 3 years for the (top row) NSA and (bottom row) TWP ARM sites with number of samples and AK sum rows (leftmost), AK application (middle left), 100 level statistics (middle right), and ~1 km slab layer statistics (rightmost). In three rightmost panels, biases (solid) are overlaid with 2σ bias uncertainty (dotted) and RMS (dashed). Gray shaded boxes cover range of possible water vapor contamination of the RO dry temperature product.

due to initialization/background errors of RO temperatures. Table 2 shows the average bias and RMS for the altitude range of 40 hPa to 100 hPa, and Figure 3 graphs the bias values with 95% confidence intervals.

5.2. Tropical Western Pacific Site

Figure 2 (bottom row) shows the TWP ARM site statistical comparisons. Due to the TWP site's location at low latitudes where polar orbiting satellites pass overhead less frequently, as well as the fact that it stopped operating at the end of 2014, this site yields only 14 matchup cases. This is evident in the larger uncertainty range for each bias profile estimate. Even with the low sample numbers, a characteristic bias of the NUCAPS retrieval within tropical regions (supported in later analyses) is seen in the 101 level and 1 km layer result—that of a negative bias at ~100 hPa accompanied by a positive bias at ~50 hPa, which implies a disagreement in the height of the tropopause. This bias feature is removed after AK application, and the RMS is reduced to 0.5 K within the 140–40 hPa range. COSMIC is seen to agree with ARM sondes from 40 to 100 hPa but with large statistical uncertainty. Table 1 and Figure 3 summarize the average bias results and show that the NUCAPS temperature agrees with the radiosondes within the uncertainty interval at the TWP site.

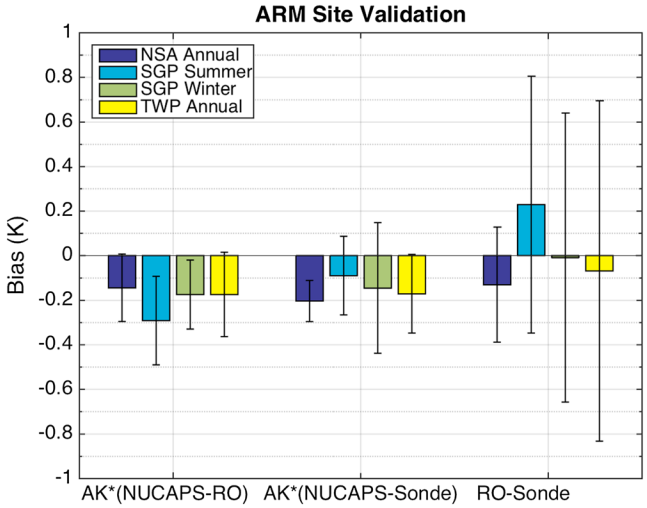

Figure 3. Chart of Table 1 bias averaged over the 40 hPa to 100 hPa altitude range for ARM sites (colored bars) overlaid with 2σ uncertainty in the bias (thin, black error bars). The NUCAPS-RO and NUCAPS-Sonde estimates include smoothing by NUCAPS averaging kernels, while the RO-sonde comparison has not been vertically smoothed.

5.3. Southern Great Plains Site

Figure 4 includes two sets of panels of statistics over the Southern Great Plains ARM site. For this site statistics were split into two different time periods whose atmospheric temperature structures were found to be similar—the months of May through September in Figure 4 (top row) and November through March in Figure 4 (bottom row). From ~200 to 30 hPa COSMIC is seen to agree with the radiosondes within the estimated 2σ bias uncertainty for both time periods. Also, similar across the two time periods is that after AK application, NUCAPS agrees with the radiosondes and COSMIC between 200 and 20 hPa and RMS values are decreased to below 1 K. In the 1 km layer and 101 level results, NUCAPS bias to the ARM sondes varies across the time periods—the summertime month bias varies less with height, staying closer to zero than the bias in wintertime months, which oscillates from +1 and −1 K between the 200 and 30 hPa pressure levels. The average bias in the 40 hPa to 100 hPa range is given in Table 1 and Figure 3.

6. NUCAPS and COSMIC Global Zonal Comparisons

6.1. Seasonal, Zonal Profile Statistics

Figures 5 and 6 show seasonal, zonal bias and RMS profile statistics for CrIS NUCAPS, AIRS ASTv6, and IASI EUMv6 overlaid for each vertical averaging case. The sum of the AK rows is also shown and serves as a guide for interpretation of the results—where the sum is closer to 1.0, the AK smoothed differences are more influenced by the RO profile. Alternatively, where the sum tends toward zero, the difference between the sounder and RO profile tends toward zero as well, which is not a sign of higher agreement but a lack of sensitivity in these levels. Plots are zoomed to the 200–10 hPa region, which again bounds the levels where COSMIC and current RO processing techniques are claimed to be of highest accuracy for the dry temperature products (which roughly ranges from ~35 hPa down to the upper troposphere). Quick comparison of the statistics over seasons and zones illustrates the range of characteristics that can be identified within specific temporal and spatial domains; however, the variance of the statistics over time and latitude is detailed in later figures. For a guide and due to their small magnitudes, the average of the AK smoothed biases and bias uncertainties over the 40–100 hPa and 15–40 hPa range are shown in Tables 3 and 4, respectively.

Upon comparing the AK smoothed and 101 level results (the middle two panels of the four panel groups), the AK application is seen to reduce the bias error for all zones, seasons, and IR sounders to within ~ ±0.5 K with exceptions for various polar zones, such as the June-July-August/March-April-May (JJA/MAM) Antarctic and December-January-February (DJF) Arctic zones. AK smoothed RMS are reduced the most from the 101 level result for altitudes below ~30 hPa. The ~1 km slab averaging also overall reduces the RMS, generally within the 40–150 hPa region but less than the application of AKs. The 1 km layering removes smaller magnitude vertical oscillations that are confined to thinner vertical extents (e.g., JJA Northern Hemisphere (NH) midlatitudes/Arctic 100–30 hPa regions) but retains and in some cases only slightly mutes structures from large-magnitude vertical oscillations (e.g., DJF tropics/Southern Hemisphere (SH) midlatitudes and JJA Antarctic 200–10 hPa). Uncertainty of the biases is negligible due to the large number of samples (>5000 per zone) included in this zonal analysis.

RMS results for all sounders relative to COSMIC RO are quite similar, with exceptions for ASTv6 in the MAM/JJA Antarctic and NUCAPS in the DJF tropics. All AK smoothed RMS values are confined under ~1 K

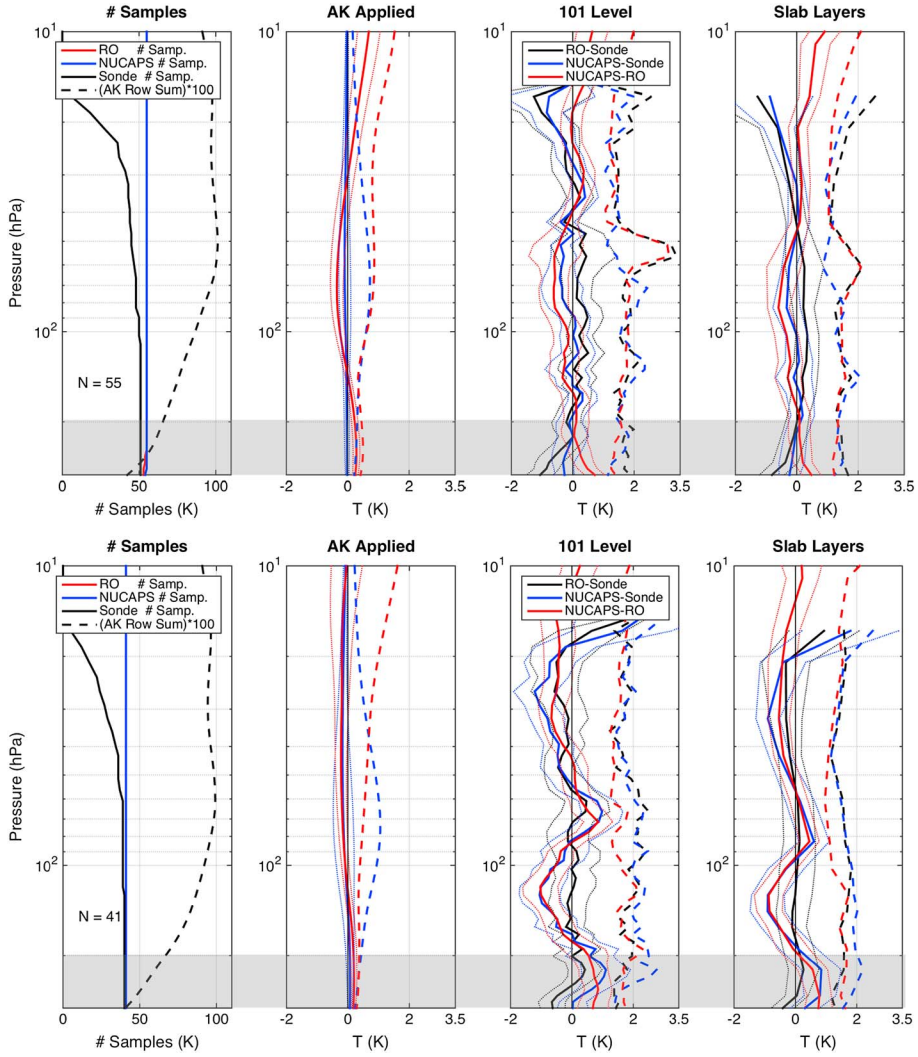

Figure 4. Same as Figure 2 except for the (top row) SGP summer (May through September) and (bottom row) SGP winter (November through March) ARM sites.

below the 40 hPa pressure level. The 101 level and 1 km layer results differ more than the AK smoothed results between zones and seasons; however, typically, for midlatitudes and polar regions RMS values reach a minimum of under 1.5 K around 60 hPa and for the tropics have a local maximum at ~70 hPa which is surrounded by 2 local minima.

Overall, the AK smoothed NUCAPS bias is well behaved, staying under or not far from ~0.25 K below 30 hPa. The 1 km layer NUCAPS bias points to the MAM/DJF tropics as the region of largest differences, and polar winter zones also exhibit larger 1 km layer biases. The EUMv6 bias performs well—even in the 101 level and ~1 km layer results the bias is seen to be within ~0.25 K more often than it is not. EUMv6 RMS for all vertical smoothings is seen to be consistent—there are no months or zones with outlying RMS values. The ASTv6 AK smoothed bias is similarly well behaved except for DJF Arctic and JJA Antarctic where it reaches above 1 K. The JJA/MAM Antarctic zone 101 level results point to an unphysical, large vertical oscillation present in the ASTv6 temperature profiles.

6.2. Monthly, 5° Zonal Results

Figure 7 shows monthly, 5° zonally averaged AK smoothed biases for two pressure levels extending from the lower stratosphere to the upper troposphere region—at ~65 and 100 hPa. The 101 level results for these pressure levels are shown in supporting information Figure S1, while results for the ~35 hPa, middle

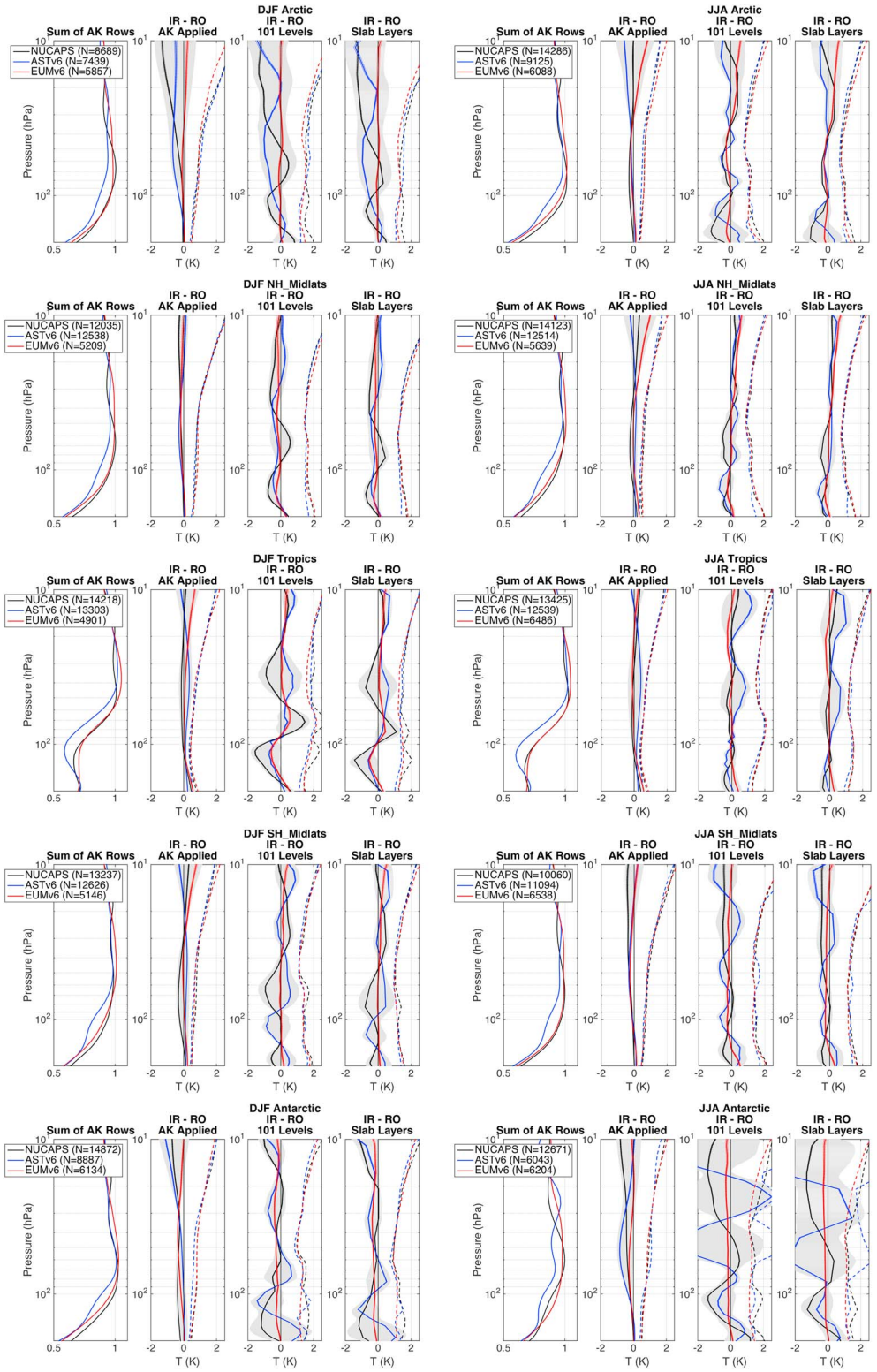

Figure 5. Seasonal, zonal IR sounder minus COSMIC bias, and RMS for NUCAPS, ASTv6, and EUMv6. Average sum of AK rows (leftmost of four panel group) and IR-RO bias (solid) with 2σ uncertainty (dotted, considered negligible) and RMS (dashed) after AKs application (second leftmost), no vertical smoothing (second rightmost), and ~1 km layering (rightmost) for five zonal regions for (left column) DJF and (right column) JJA seasons. Gray shading marks area under ±2 standard deviations from the mean of the three IR sounder biases and provides a measure of the average IR sounder accuracy compared to COSMIC RO.

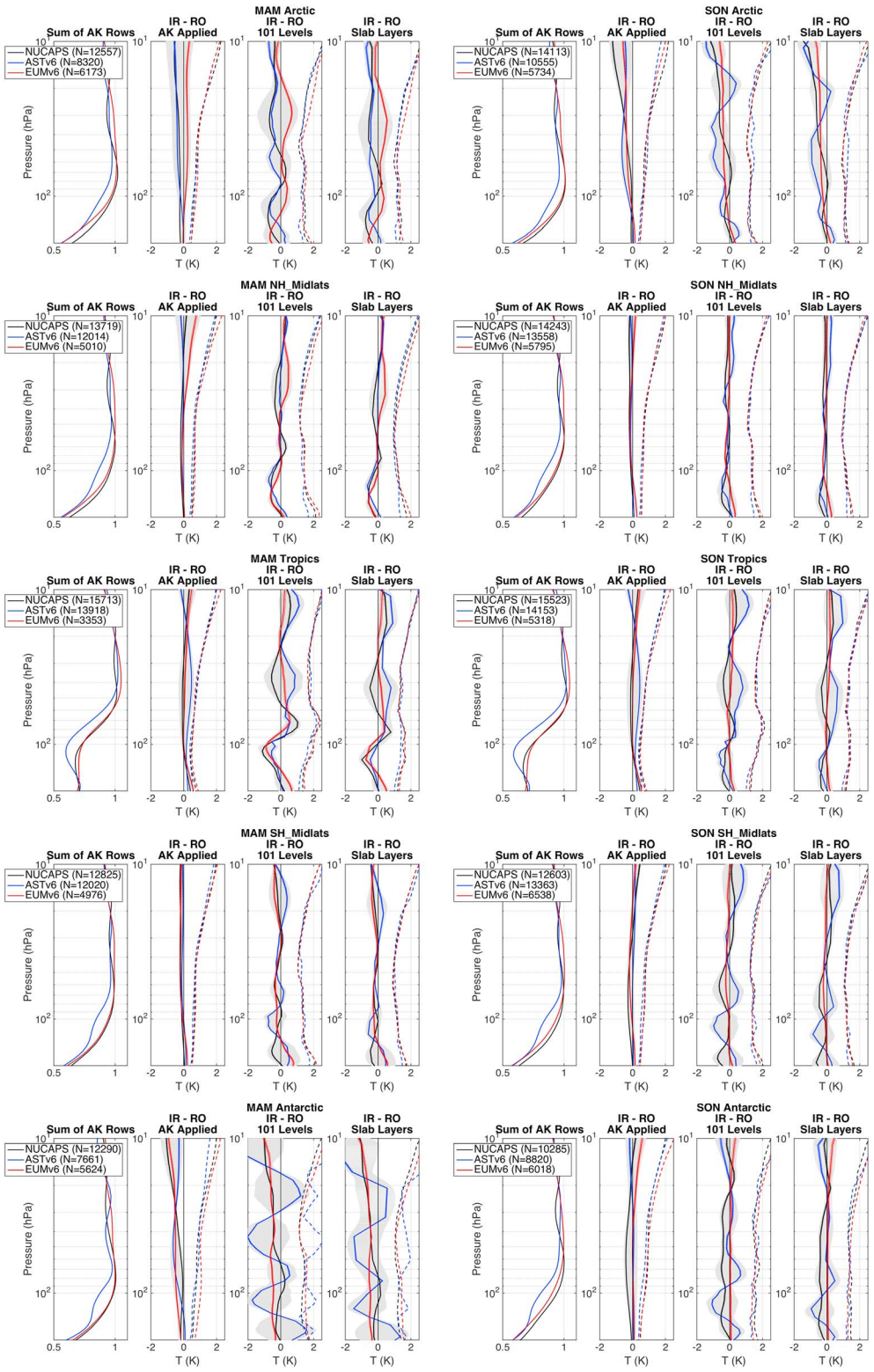

Figure 6. Same as Figure 5 except for (left column) MAM and (right column) SON seasons.

stratospheric pressure level, are shown in supporting information Figure S2. These three pressure levels are selected from vertical regions where the AK row sum is close to 1.0 across all zones (with exceptions for the 100 hPa tropical region where the AK sum drops down to 0.6). Due to the smaller number of samples on the monthly, 5° zonal scales, the bias uncertainty is larger and results are only shown for regions where

Table 3. Seasonal, Zonal AK*(IR Sounder Minus COSMIC) Bias and 1σ Bias Uncertainties Averaged Over the Vertical Range of 40 to 100 hPa

AK*(IR-RO) Bias, 1σ Uncertainty, and RMS 40–100 hPa Average

	DJF			MAM			JJA			SON		
	Bias	Unc	RMS	Bias	Unc	RMS	Bias	Unc	RMS	Bias	Unc	RMS
						NUCAPS						
90°N–60°N	−0.228	0.00909	0.885	−0.238	0.00628	0.743	−0.241	0.00517	0.665	−0.180	0.00578	0.717
60°N–30°N	−0.130	0.00713	0.794	−0.173	0.00556	0.674	−0.173	0.00508	0.631	−0.169	0.0056	0.69
30°N–30°S	−0.111	0.00489	0.594	−0.072	0.00503	0.634	−0.103	0.00485	0.572	−0.102	0.00493	0.623
30°S–60°S	−0.266	0.00624	0.768	−0.159	0.00596	0.694	−0.218	0.0078	0.815	−0.243	0.00643	0.763
60°S–90°S	−0.335	0.006	0.807	−0.153	0.00702	0.798	−0.340	0.00701	0.86	−0.372	0.00801	0.894
						ASTv6						
90°N–60°N	−0.539	0.00906	0.951	−0.322	0.00759	0.764	−0.095	0.00546	0.531	−0.522	0.00595	0.807
60°N–30°N	−0.238	0.00653	0.77	−0.081	0.0052	0.576	0.109	0.00468	0.535	−0.096	0.00529	0.624
30°N–30°S	0.222	0.00427	0.541	0.321	0.00439	0.61	0.283	0.00432	0.561	0.319	0.00437	0.61
30°S–60°S	0.161	0.00531	0.618	−0.083	0.00572	0.634	−0.245	0.00652	0.731	0.0036	0.00547	0.633
60°S–90°S	−0.075	0.00621	0.592	−0.509	0.00737	0.826	−0.661	0.00836	0.931	0.0467	0.00757	0.713
						EUMv6						
90°N–60°N	−0.0724	0.0119	0.915	0.195	0.0105	0.845	−0.127	0.00842	0.67	−0.283	0.00946	0.773
60°N–30°N	−0.147	0.0119	0.871	−0.0669	0.00985	0.702	0.0047	0.00747	0.562	−0.129	0.00847	0.659
30°N–30S	0.0421	0.00778	0.547	0.0224	0.0108	0.628	−0.044	0.00703	0.568	−0.0028	0.00876	0.639
30°S–60°S	−0.0122	0.00936	0.673	−0.169	0.0101	0.735	−0.216	0.00889	0.752	−0.138	0.00895	0.738
60°S–90°S	−0.276	0.00951	0.796	−0.492	0.0123	1.04	−0.228	0.01	0.824	0.0182	0.0113	0.877

the uncertainty of the bias is less than the bias difference itself. Characteristic spatiotemporal patterns are revealed across time and latitude as evident features are repeated from year to year for ASTv6 and NUCAPS, e.g., the cold bias in ASTv6 polar winter months at 35 hPa or the NUCAPS 65 hPa January warm and cold bias at 20 −50° latitude, respectively. While the AK smoothed biases for all IR sounders are qualitatively similar across all pressure levels, the 101 level biases are different between heights.

NUCAPS AK smoothed bias is often under the uncertainty estimate in the tropical regions and is otherwise dominantly below 0.5 K at all levels (seen by lack of thin black contours denoting 0.5 K increments). An interesting feature of the 101 level bias in the tropics/NH midlatitude occurs around January–March where a strong warm bias at 65 hPa turns into a strong cold bias at 35 hPa. This is also seen in the above profile

Table 4. Same as Table 2 Except for the 15 to 40 hPa Vertical Range

AK*(IR-RO) Bias, 1σ Uncertainty, and RMS 40–100 hPa Average

	DJF			MAM			JJA			SON		
	Bias	Unc	RMS	Bias	Unc	RMS	Bias	Unc	RMS	Bias	Unc	RMS
						NUCAPS						
90°N–60°N	−0.802	0.0166	1.74	−0.397	0.0111	1.31	−0.0566	0.00851	1.02	−0.678	0.00962	1.33
60°N–30°N	−0.24	0.0127	1.42	−0.0483	0.00965	1.13	0.102	0.0091	1.09	−0.186	0.00985	1.19
30N–30°S	−0.0593	0.0097	1.16	0.0491	0.00944	1.19	0.0745	0.00932	1.08	0.0273	0.00935	1.17
30°S–60°S	0.0424	0.0101	1.17	−0.188	0.0103	1.19	−0.379	0.0139	1.45	0.0433	0.0106	1.19
60°S–90°S	−0.379	0.00959	1.23	−0.59	0.0102	1.28	−0.498	0.0103	1.26	−0.173	0.0116	1.2
						ASTv6						
90°N–60°N	−0.547	0.0198	1.8	−0.439	0.0133	1.29	−0.303	0.00968	0.973	−0.487	0.0101	1.16
60°N–30°N	−0.0644	0.0126	1.42	−0.0341	0.00974	1.07	0.0791	0.00924	1.04	−0.0522	0.00969	1.13
30°N–30°S	0.236	0.00973	1.16	0.332	0.00954	1.19	0.293	0.00939	1.11	0.284	0.00939	1.17
30°S–60°S	0.0968	0.00985	1.12	−0.0543	0.01	1.1	−0.149	0.0125	1.33	0.122	0.0097	1.13
60°S–90°S	−0.465	0.0111	1.14	−0.437	0.0121	1.16	−0.374	0.0143	1.21	−0.0195	0.0123	1.16
						EUMv6						
90°N–60°N	0.0951	0.0186	1.43	0.207	0.016	1.27	0.154	0.0143	1.14	−0.408	0.015	1.21
60°N–30°N	−0.122	0.0197	1.43	0.247	0.0168	1.22	0.319	0.0135	1.07	−0.0414	0.0148	1.13
30°N–30°S	0.24	0.016	1.15	0.168	0.0205	1.2	−0.0388	0.0138	1.11	0.141	0.017	1.25
30°S–60°S	0.172	0.0166	1.21	−0.199	0.0167	1.19	−0.102	0.017	1.38	−0.0732	0.0151	1.23
60°S–90°S	−0.238	0.0148	1.19	−0.566	0.0175	1.43	−0.0317	0.0157	1.24	0.164	0.0175	1.37

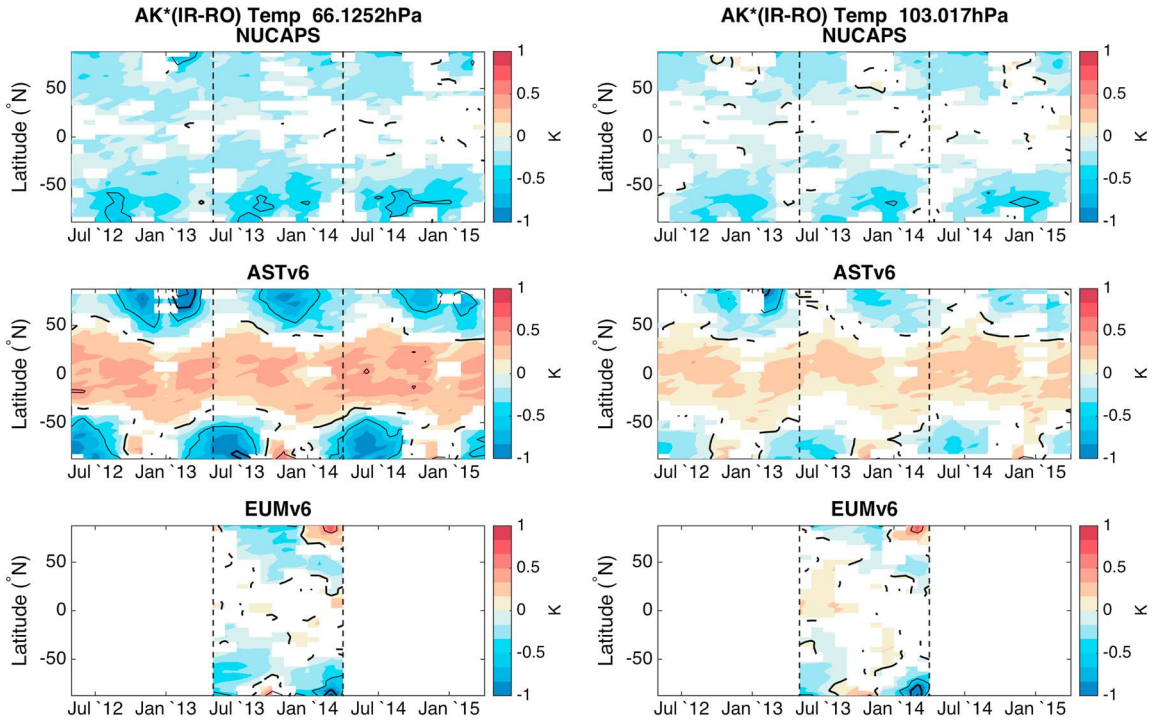

Figure 7. Monthly, 5° zonally averaged results. AK smoothed IR minus COSMIC biases for (top row) NUCAPS, (middle row) ASTv6, and (bottom row) EUMv6 for the ~65 hPa level (left column) and ~100 hPa level (right column). Contours are shown for every 0.5 K (thin) and 1 K (bold).

statistics—both the seasonal MAM/DJF tropical zones and the comparison of NUCAPS against radiosondes at the TWP ARM site.

At 35 hPa, ASTv6 AK smoothed result has a warm bias in the tropical region which reaches over 0.5 K in various regions and a cold bias in polar winter months that reaches under −0.5 K. This pattern is consistent with the 101 level results, though the magnitudes are larger in the 101 level bias. The AK smoothed bias pattern at 35 hPa is also seemingly carried down through the atmosphere to both the 65 and 100 hPa levels, decreasing to magnitudes of less than ~0.25 K. The largest magnitudes of the 101 level biases seen in the lower latitudes at all three levels show the temporal and latitudinal extent of the unphysical ASTv6 vertical oscillation reflected in the seasonal statistics above.

EUMv6's AK smoothed bias, somewhat similar across heights, is almost everywhere under 0.5 K magnitude. The 101 level results are dominantly under 1 K with exceptions seemingly clustered closer to tropical latitudes.

6.3. Time Series

To highlight the IR-RO differences seasonal dependence and to facilitate a more direct comparison of the IR sounder performances, Figure 8 shows zonal time series of the AK smoothed results at the ~65 hPa level, while Figure S3 shows results for the 101 level results. Time series are obtained by lowess filtering daily mean values to remove outliers. The typical number of samples is ~50 per day for each of the five latitude zones; however, the number varies regularly from ~10 to 100 in some regions such as the tropics, which calls for caution in interpretation of the results. Also overlaid with the daily means in Figure 8 are the daily mean ±2 daily mean uncertainties as faint colored lines.

Seasonal patterns are seen in the polar and midlatitude 101 level and AK smoothed temperature differences; however, they are of lesser magnitudes in the AK smoothed results. The tropical zone 101 level differences also contain seasonal patterns, but they are removed by the AK application. The AK smoothed differences are often under 0.5 K and are within or not far from the estimated 2σ uncertainty of the mean, with an exception for ASTv6 divergences in the polar regions around wintertime. In the tropical zone, AK

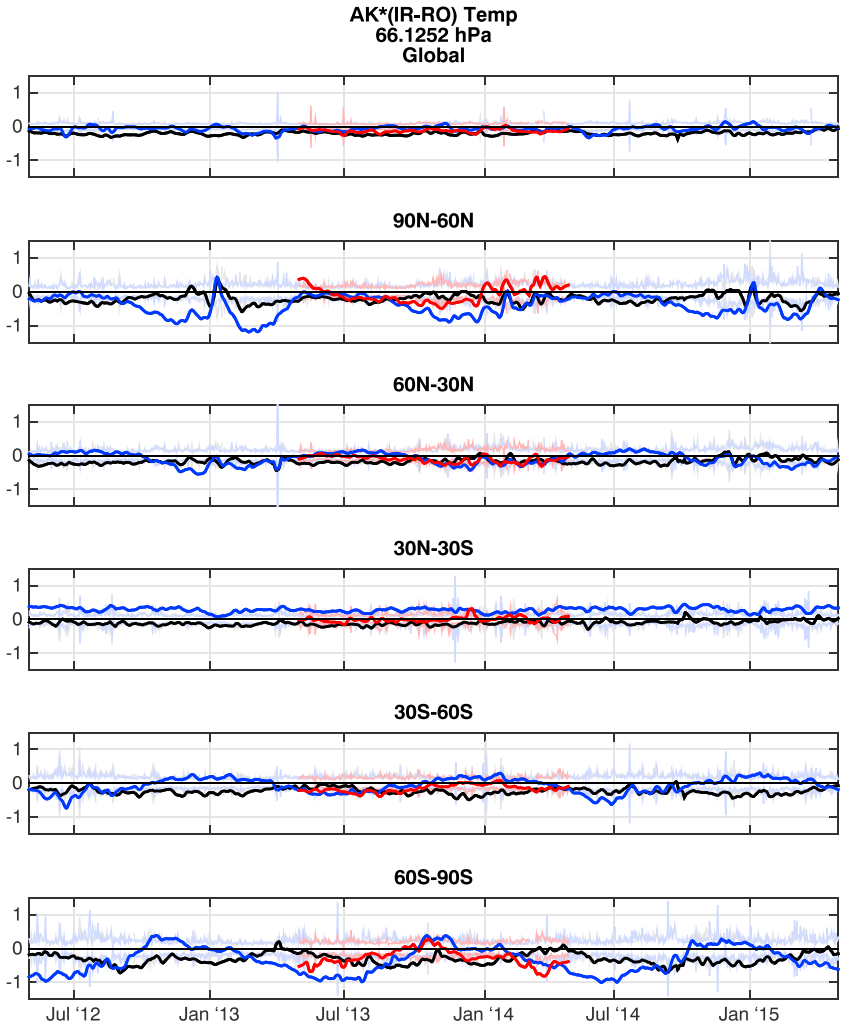

Figure 8. Time series of AK*(IR − RO) temperature differences at ~65 hPa. Lowess-filtered daily means of differences (bold) and daily mean ±2 daily mean uncertainties (light colors) overlaid for NUCAPS (black), ASTv6 (blue), and EUMv6 (red) for a global (top) and all latitude zones.

smoothed results are consistently around 0 K for EUMv6, −0.1 K for NUCAPS, and 0.3 K for ASTv6, with ASTv6, in general, being outside the 2*daily uncertainty range.

EUMv6 AK smoothed differences are most outside their uncertainty range in the Antarctic June and March time frames, where they briefly reach under −0.5 K, which is consistent with the 101 level results. The obvious spurious ASTv6 and NUCAPS temperature difference feature in the Arctic following January 2013 is seen in both smoothing of temperatures. The number of matchups for both ASTv6 and NUCAPS in this time period are seen to be under 20 for an extended period of time, which may be having an influence on the bias if the matchup spatiotemporal sampling is not consistent with time. Temperature profiles and their differences for this zone during January and February are shown in supporting information Figures S4 and S5 and reveal a change in atmospheric structure between the 2 months which could be a cause of the spurious differences. Figure S6 shows time series of differences for the ~35 and ~103 hPa pressure levels and illustrate both the variance of the differences across height in the 101 level results and the similarity in the structure of the time series across height in the AK smoothed results.

From the summary results of Table 3 for the 40 hPa to 100 hPa average bias we can compute a double difference between NUCAPS-COSMIC and ASTv6-COSMIC to estimate the 30° zonal latitude difference between NUCAPS and ASTv6. A similar double difference with EUMv6-COSMIC yields the mean zonal bias between NUCAPS and EUMv6 temperatures. Figure 9 shows the double difference comparison of NUCAPS

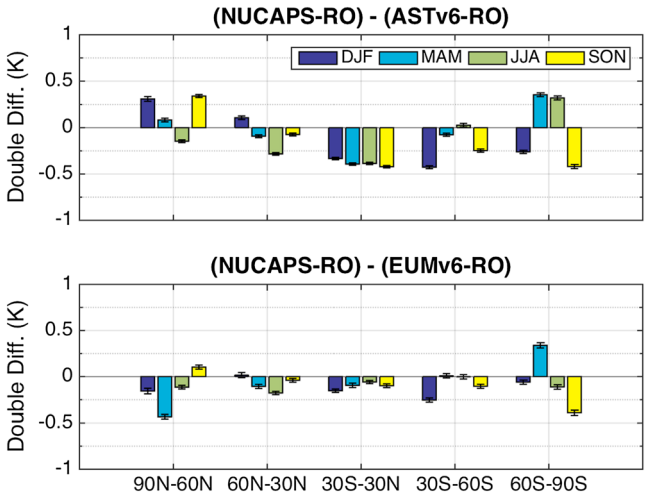

Figure 9. Double difference of (top) NUCAPS-COSMIC minus ASTv6-COSMIC and (bottom) NUCAPS-COSMIC minus EUMv6-COSMIC for the 40 hPa to 100 hPa vertical range after application of averaging kernels. Error bars about the end of the bars are the RSS of 2*NUCAPS bias uncertainty and 2*ASTv6 bias uncertainty in Figure 9 (top) and the RSS of 2*NUCAPS bias uncertainty and 2*EUMv6 bias uncertainty in Figure 9 (bottom). Values are computed from Table 2.

with ASTv6 and with EUMv6 separated by season. Excluding the polar regions, NUCAPS appears to agree slightly better with EUMv6 than with ASTv6. In particular, a systematic NUCAP minus ASTv6 bias of about −0.3 K to −0.4 K is found in the tropical zone, whereas the bias of NUCAPS with EUMv6 is less than 0.2 K. Overall, the NUCAPS temperature in the 40 hPa to 100 hPa range is within 0.5 K of both ASTv6 and EUMv6 for all latitude zones, after application of the corresponding averaging kernels.

7. Discussion and Conclusions

The objective of this work was to assess the NOAA NUCAPS temperature profile product from the upper troposphere through the middle stratosphere and to characterize seasonal and latitudinal systematic biases and root-mean-square errors. Vaisala RS92 radiosondes launched from fixed ARM sites are used as a temperature absolute reference but are limited statistically by the number of time and space coincident samples. A comparison of NUCAPS with COSMIC RO provides a statistically large data set on 30° latitude zones for each of the four seasons. The relative stability of the UCAR COSMIC dry temperature product allows it to be used as a common reference for the intercomparison of NUCAPS temperature products to similar products produced by NASA from Aqua AIRS and by EUMETSAT from MetOp-B IASI.

To provide an objective assessment of the IR sounder retrieval products, averaging kernels were calculated from temperature Jacobians obtained from the OSS radiative transfer model. Application of the averaging kernels to the IR sounder minus RO and IR sounder minus ARM radiosonde differences significantly decreased the magnitude of the biases. The RMS error was also dramatically reduced by the AK smoothing. In contrast, the ~1 km slab layering described in the paper only slightly decreased the bias and RMS values and largely retained the systematic vertical oscillation features seen in the 101 level results. The averaging kernels and ~1 km slab layering characterize different types of errors and should both be used to investigate difference errors (e.g., see ASTv6 Antarctic results). The results of this paper suggest that IR vertical averaging kernels need to be computed and applied consistently among the radiosonde, RO, and IR sounding differences on a case by case basis, and they support the motivation for data centers to supply users with averaging kernels.

Time and space coincident matchups of DOE ARM radiosondes with NUCAPS and COSMIC temperature profiles were found over a period of 3 years at the NSA, SGP, and TWP sites. The NUCAPS profiles used in the resulting three-way comparison were computed using an averaging method that matches the IR profile resolution to that of the COSMIC RO profile and accounts for the horizontal averaging effects of the RO. This method thus reduces spatiotemporal mismatch error between the NUCAPS and COMSIC RO profiles. Vertical averaging is also applied to all three comparisons to account for the different vertical resolutions of the radiosonde, COSMIC RO, and IR sounder profiles in the 100 to 40 hPa range. The ARM site analysis

finds the NUCAPS temperature in this pressure range to have an average bias to the radiosondes of less than 0.44 K and an RMS error of less than 1 K. In particular, as seen in Table 2, the average NUCAPS bias and RMS error relative to radiosondes is found to be −0.20 ± 0.09 K (0.70 K RMS) for the NSA, −0.09 ± 0.18 K (0.66 K RMS) for SGP summer, −0.15 ± 0.29 K (0.95 K RMS) for SGP winter, and −0.17 ± 0.18 K (0.37 K RMS) for TWP. Relative to COSMIC RO, NUCAPS bias is −0.14 ± 0.15 K (1.10 K RMS) for the NSA, −0.29 ± 0.20 K (0.80 K RMS) for SGP summer, −0.17 ± 0.16 K (0.53 K RMS) for SGP winter, and −0.17 ± 0.19 K (0.41 K RMS) for TWP. The uncertainties stated above represent the 95% confidence interval ($k = 2$).

Three years of Suomi-NPP CrIS and Aqua AIRS matchups to COSMIC RO are used to calculate IR sounder minus COSMIC bias and RMS statistics in five global latitude zones. A similar matchup analysis was performed with 1 year of MetOP-B IASI data. The comparison of CrIS/NUCAPS to EUMETSAT IASI version 6 and NASA AIRS version 6 temperature products could reveal biases in the calibrated radiances. Direct comparison has been made between CrIS and IASI and AIRS radiances using simultaneous nadir overpasses [*Tobin et al.*, 2013]. In this study, the double difference between NUCAPS-COSMIC and ASTv6-COSMIC provides some information about the CrIS and AIRS brightness temperature observations as they are used by the corresponding retrieval algorithms. NUCAPS agreement with ASTv6 and EUMv6 is less than 0.5 K after application of averaging kernels for the vertical range of 100 to 40 hPa. The results are only slightly worse in the 40 to 15 hPa region of the middle stratosphere. For altitudes above the 15 hPa pressure level, the uncertainties in the COSMIC RO dry temperature product preclude making firm conclusions.

Further work will involve comparison with official GRUAN processed temperature soundings from the ARM sites. The use of RO has been shown to be a powerful method for intercomparison of satellite soundings from different sensors using different algorithms sampling different times of day. Routine comparison of future operational RO, dedicated radiosondes, hyperspectral IR, and advanced microwave soundings is recommended to help understand systematic errors inherent in each observing approach.

Appendix A: Vertical Averaging Techniques

A1. Averaging Kernel Calculations

When it is assumed that the RO represents the "true" atmospheric state and no vertical smoothing is applied, the RO and IR sounder temperature difference statistics provide an assessment of the IR sounder measuring system's ability to capture the true atmospheric state; however, they do not account for the inherently more limited capability of the IR sounders to resolve atmospheric structures in the vertical. To provide a fair assessment of the retrieval scheme by accounting for the theoretical measuring capabilities of the IR sounders, averaging kernel (AK) matrices are used [*Rodgers and Connor*, 2003; *Rodgers*, 1990]. AK matrices are smoothing functions that replicate the smoothing induced by the vertical integral inherent in the IR radiative transfer equation and ideally represent the radiance sensitivity to temperature to nearby heights of the atmosphere [*Luo et al.*, 2007], and they are applied to the higher-resolution profiles to decrease their resolution to that of the IR sounder.

For this work, AIRS, CrIS, and IASI instrument AKs are calculated and applied to the RO/IR sounder matchup temperature differences for each individual matchup, with the AK application denoted as AK* in the figures. Temperature Jacobians, also referred to as weighting functions (WFs), required for the AK calculations are calculated using the OSS RTM [*Moncet et al.*, 2008] for the subset of channels listed in Table A1. CrIS temperature Jacobians are calculated for unapodized radiances, and for the 15 μm region subset of channels, the unapodized CrIS AKs are qualitatively similar to the AKs computed from IASI and AIRS (shown in following Figure A3). For each matchup case RTM calculation, atmospheric parameters of ozone, water vapor, skin temperature, and surface pressure from the ERA-Interim reanalysis, carbon dioxide from NOAA's CarbonTracker, and the IR sounder-retrieved temperature profile and instrument scan angle are used as input to the RTM.

In the following description of the AK calculation and application process, vectors are denoted by lowercase bold font and matrices by uppercase bold font. The temperature Jacobian, $\mathbf{K}$, is defined by $\mathbf{K} = (\mathbf{x} - x_o)/(\mathbf{y} - y_\mathbf{o})$, where $\mathbf{x}$ is the true atmospheric temperature profile, $\mathbf{y}$ is the top of atmosphere radiance, and $f(\mathbf{x})$ is the forward model defined as $\mathbf{y} = f(\mathbf{x})$ which is linearized about $(x_o, y_\mathbf{o})$ and neglects instrument measurement error [*Rodgers and Connor*, 2003]. $\mathbf{K}$ thus describes the portion of the temperature profile represented by each radiance measurement [*Rodgers*, 1976]. Figure A1 illustrates the IASI, AIRS, and CrIS temperature

Table A1. IASI, CrIS, and AIRS Channels Selected for Use in the AK Calculation

		IR Instrument Channel Definition
IASI	Chan (#)	26, 38, 39, 49, 57, 88–100, 105, 106, 108, 109, 173, 186, 195, 210–212
	cm^{-1}	651.25, 654.25, 654.50, 657.00, 659.00, 666.75–669.75, 671.00, 671.25, 671.75, 672.00, 688.00, 691.25, 693.50, 697.25–697.75
CrIS	Chan (#)	8, 18, 21, 26, 28–33, 35, 36, 51, 52, 57, 70, 75, 77
	cm^{-1}	654.375, 662.500, 660.625, 665.625, 666.875–670.000, 671.250, 671.875, 681.25, 681.875, 685.000, 693.125, 696.250, 697.500
AIRS	Chan (#)	9, 34, 69–83, 88, 89, 91, 92, 128, 150, 156, 162, 168, 169
	cm^{-1}	651.5329, 657.5886, 666.2706–669.8116, 671.0859, 671.3414, 671.8530, 672.1091, 681.4665, 692.7567, 694.4010, 696.0533, 697.7136, 697.9911

Jacobians computed by OSS for the sets of channels used in the AK calculations, which are listed in Table A1. The AIRS channel set used for this study contains the channels suggested by *Hoffmann and Alexander* [2009] for use in stratospheric temperature retrievals. Channels from the 15 μm CO_2 absorption region are chosen for each instrument with the following criteria: their WF has a well-defined peak between 1 and 300 hPa and the integrated weights of their WF between 1 and 300 hPa is maximized. To calculate the AKs after the **K** matrices are obtained, a Tikhonov regularization approach is used to condition the inverted matrix $\mathbf{K}^T\mathbf{K}$ in the equation which defines the averaging kernel, **A**, as follows:

$$\mathbf{A} = \left(\mathbf{K}^T\mathbf{K}+\gamma\mathbf{I}\right)^{-1}\times\mathbf{K}^T\mathbf{K}, \tag{A1}$$

where **I** is the identity matrix and γ is a constant used to condition the matrix $(\mathbf{K}^T\mathbf{K})^{-1}$. For every matchup case's computed **K** matrix, equation (A1) is used to calculate the corresponding AK. Also referred to as a damping parameter, γ in this study is also calculated for each matchup case using singular value decomposition on the inverted matrix, $\mathbf{K}^T\mathbf{K}$. To ensure that the determined gamma value conditions the inverse matrix properly, the condition number, which is the ratio of the largest to smallest singular value, is calculated as well. The closer to 1 the condition number is, the more well conditioned the matrix is. The constant γ in this analysis is defined as the leading eigenvalue following the eigenvalue corresponding to retaining at least 99% of the inverted matrix information. In other words, the eigenvalue corresponding to retaining 99% of the information is found and the following eigenvalue is selected. While variations are seen with instrument and stratospheric lapse rate, gamma is typically defined as the fourth leading eigenvalue, which makes sense since the number of retained eigenvalues corresponds to how many pieces of information are present in the measurements (and IR sounders can contain up to seven pieces in their measurements and this analysis uses only a subset of the IR sounder channels).

Degrees of freedom (DOF), calculated as the trace of the AK matrix, is another way to describe information content and is shown in Figure A2 (top), which illustrates the relationship between the condition number, percent information retained, and DOF for the IASI, CrIS, and AIRS January 2014 tropical zone AKs. For this

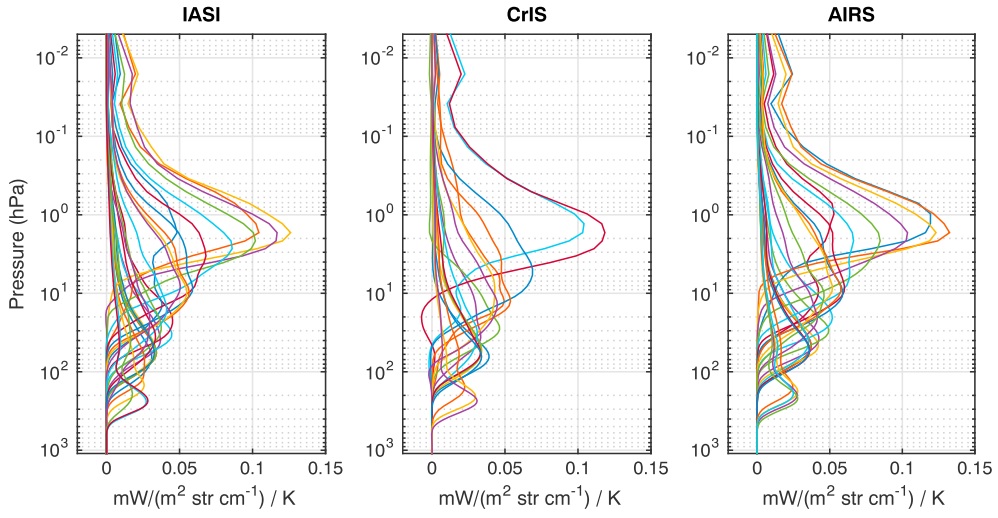

Figure A1. IASI, CrIS (unapodized), and AIRS January 2014, 30°N–30°S average temperature Jacobians illustrating the 15 μm region channels used to calculate averaging kernels.

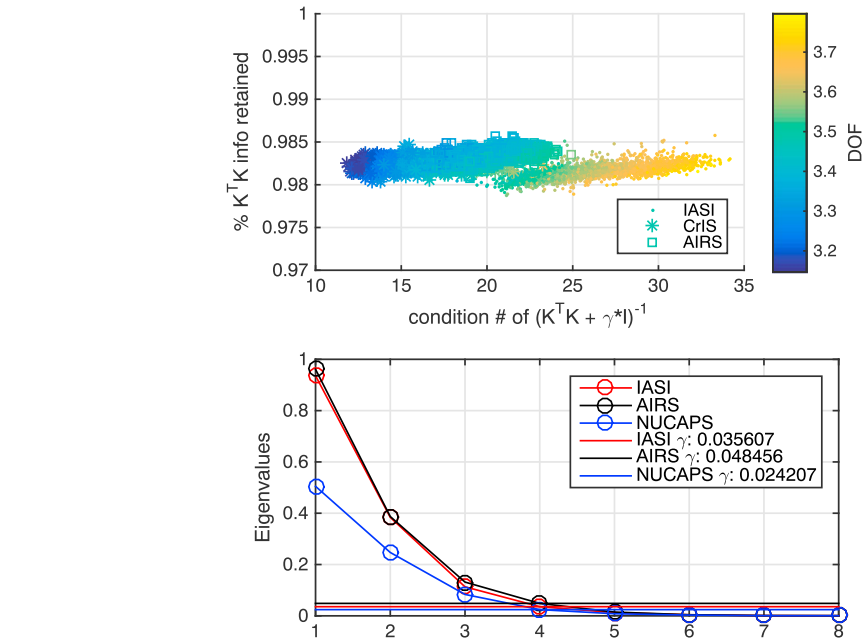

Figure A2. January 2014, 30°N–30°S AK calculation information. Percent information retained of ($\mathbf{K}^T\mathbf{K}$) versus condition number of the inverse matrix ($\mathbf{K}^T\mathbf{K} + \gamma\mathbf{I}$) colored by DOF of the (top) AK matrix and (bottom) the eight leading, monthly average eigenvalues with gamma values marked by horizontal lines and noted in the legend for AIRS, CrIS, and IASI.

subset, condition numbers are generally below 40, either four or five eigenvalues are retained (not shown), and the DOF ranges between ~3 and 5. In a pattern not exclusive to this zone and month, IASI measurements are seen to generally contain more independent pieces of information than AIRS or CrIS; however, this also causes the condition numbers for some of IASI's calculated AKs to be higher as well. Figure A2 (bottom) shows the corresponding monthly average eigenvector leading entries with horizontal lines representing the average gamma values used in the AK matrix inverse calculation. Similar to the DOF, only three to four independent pieces of information are obtained on average. Figure A2 shows that rational amounts of information are being represented in the AK calculations.

As in *Rodgers* [1990], the averaging kernel is related to true atmospheric temperature and the retrieved temperature, $\mathbf{x_{ret}}$, by $\mathbf{x_{ret}} = \mathbf{Ax} + (\mathbf{I} - \mathbf{A})\mathbf{x_o}$. From this equation, it is recognized that the sum of the AK matrix rows

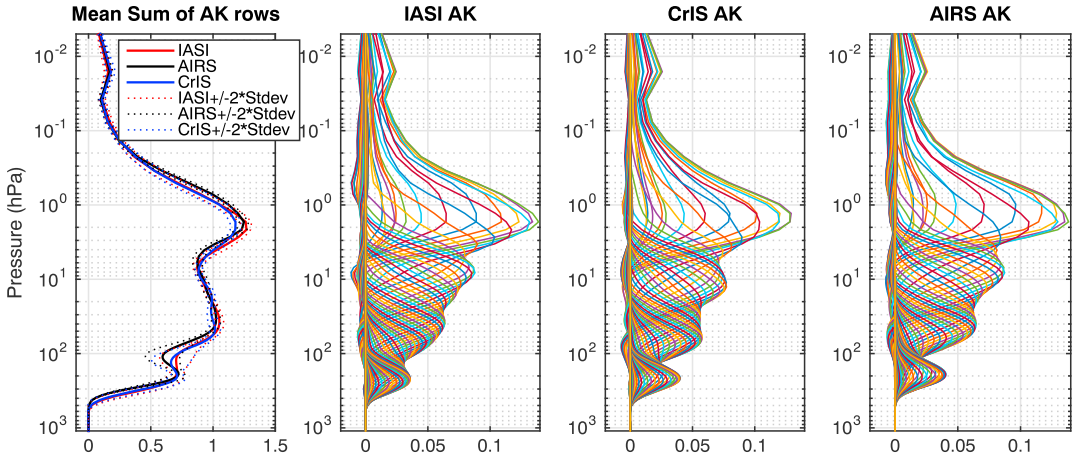

Figure A3. January 2014, 30°N–30°S mean IR sounder temperature averaging kernels. Average sum of IASI, CrIS, and AIRS AK rows overlaid with (first panel) ±2 standard deviations and average (second panel) IASI, (third panel) CrIS, and (fourth panel) AIRS averaging kernels, respectively.

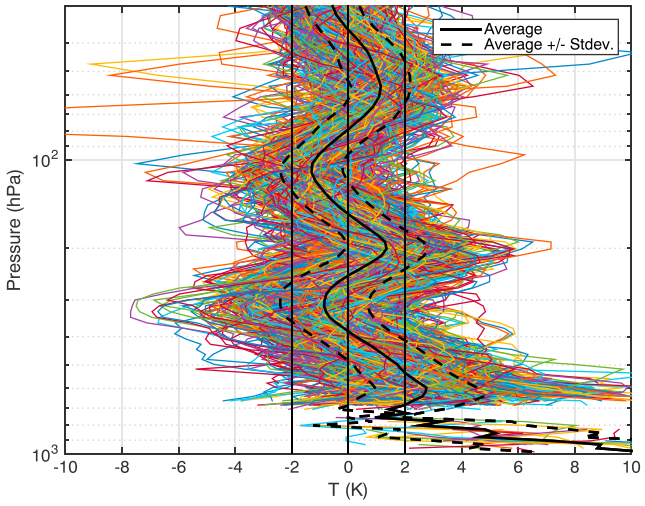

Figure A4. Effect of different vertical resolving capabilities of RO and CrIS hyperspectral IR sounder instrument in Arctic winter. January 2014 Arctic (60–90°N) matchup NUCAPS and COSCMIC temperature differences as follows, where AK* denotes the CrIS AK application: AK*(NUCAPS-COSMIC) − (NUCAPS-COSMIC) (colored profiles). Bias (solid black) and bias plus minus standard deviation (dashed black) of these differences are overlaid.

(or the areas under each of the AK curves) represents the fractional weighting applied to the true/higher-resolution profile, while the sum of the matrix **I-A** represents weighting from the reference (or a priori) profile. Figure A3 shows the average January 2014, 30°N–30°S sum of AK matrix rows and AKs for IASI, CrIS, and AIRS. While the three IR sounders have different spectral resolutions and different spectral sampling, they have very similar averaging kernels. Figure A3 (first panel) shows that for each individual AK matrix the sum of its rows does not vary from the zonal mean by more than 0.1 at the 95% confidence level, with the exception of the 80–200 hPa vertical region. The truth profile alone is dominantly contributing to AK smoothed profile difference in the 10–80 hPa region where the AK row sum is ~1.0. The width of each AK curve is a measure of the vertical resolution of the observing system [*Rodgers*, 1976]. From the previous equation defining $\mathbf{x_{ret}}$, a

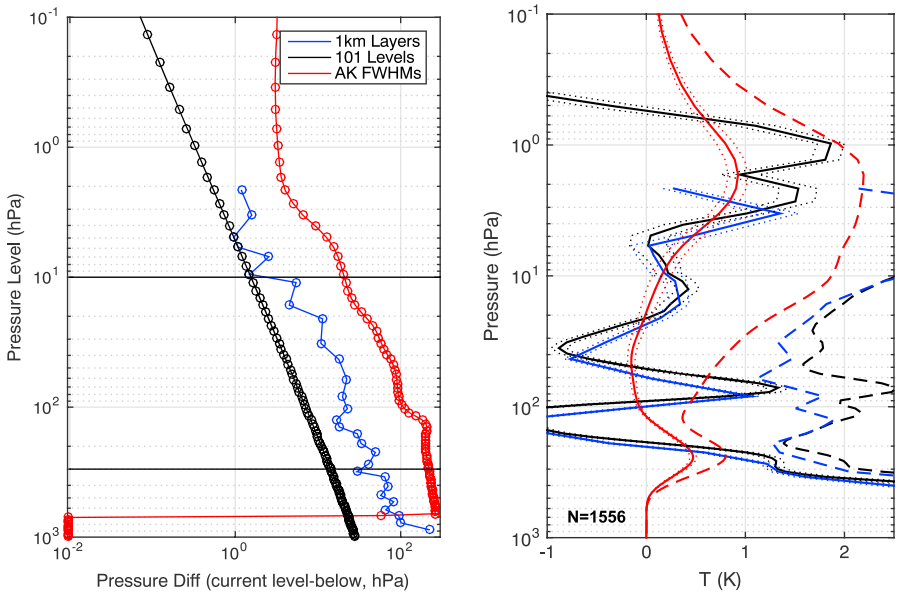

Figure A5. Comparison of different vertical smoothing applications applied to the IR sounder minus RO differences. (left) Approximate vertical resolutions as determined by the January 2014 global mean CrIS AK FWHMs (red) and pressure difference of the 1 km (blue) and 101 (black) levels below from the current levels with black horizontal lines bounding region of interest. (right) January 2014, 30°N–30°S, NUCAPS minus RO bias (solid) with uncertainty (dotted) and RMS (dashed) with no vertical averaging (i.e., on 101 levels, black), ~1 km layering (blue), and AK application (red).

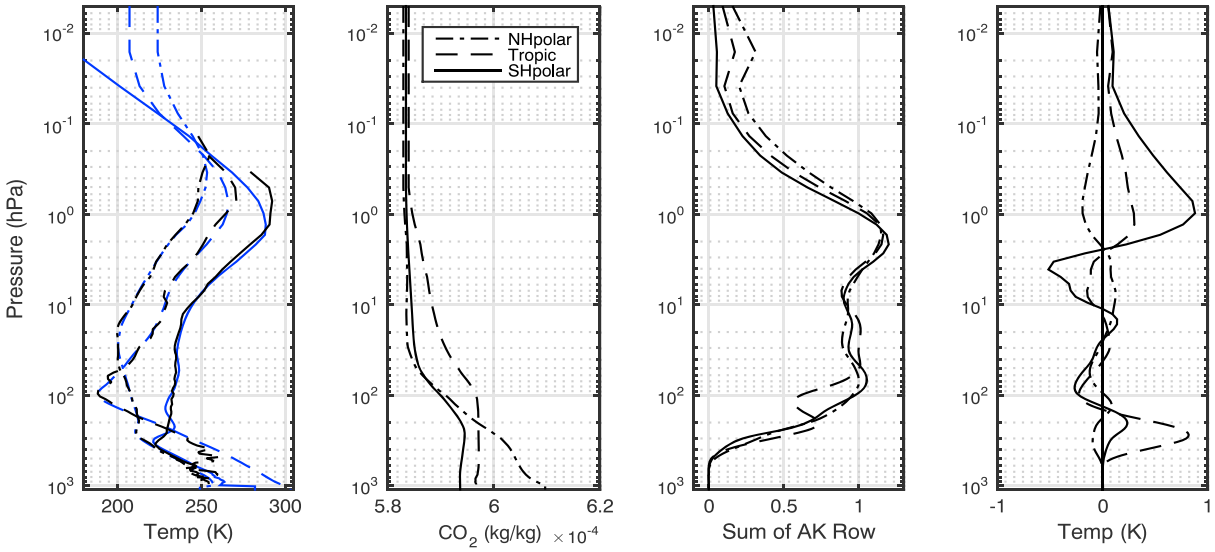

Figure A6. IR sounder instrument scan angle effect on AK smoothed IR-RO temperature differences. (first panel) NUCAPS (blue) and COSMIC (black) matchup temperatures, (second panel) carbon dioxide RTM input, (third panel) mean of scan angle 50° and 0° sum along the AK rows, and (fourth panel) difference of the AK*(NUCAPS − COSMIC) temperature difference for a scan angle of 0° and 50° (difference taken as scan angle 0 minus scan angle 50) for three cases representing different latitude zones.

smoothed version, $\mathbf{x_{smooth}}$, of a higher-resolution, "truth" profile, in this case of the RO, is calculated by $\mathbf{x_{smooth}} = \mathbf{x_o} + \mathbf{A}(\mathbf{x} - \mathbf{x_o})$ and thus the smoothed IR sounder minus RO temperature difference by [*Connor et al.*, 1994; *Rodgers and Connor*, 2003].

$$(\mathbf{x_{ret}} - \mathbf{x})_{\text{smooth}} = (\mathbf{x_{ret}} - \mathbf{x_o}) - \mathbf{A}(\mathbf{x} - \mathbf{x_o}). \tag{A2}$$

Equation (A2) is used to calculate the AK smoothed IR minus RO temperature differences, where $\mathbf{x_o}$ is defined to be the temperature profiles used to compute the Jacobians, which are the IR sounder retrievals [*Rodgers*, 1990; *Rodgers and Connor*, 2003].

The impact of applying AKs is illustrated in Figure A4 using January 2014 Arctic NUCAPS and COSMIC matchup temperature differences and corresponding CrIS AKs. The following double differences are taken between the RO and IR sounder profiles: AK*(IR-RO) − (IR-RO). Figure A4 shows the bias of the double differences with single standard deviations bounding it on each side. On average, the RO is able to resolve just over 1 K larger temperature magnitudes than the CrIS/NUCAPS observing system. As shown by the dashed standard deviation lines, 32% of the time the RO is able to resolve magnitudes over 2 K larger than the IR observing system and for some extreme profiles the RO resolves over 6 K magnitude larger temperature features.

A2. Comparison of Methods

Figure A5 compares the two different vertical averaging methods applied to IR sounder and RO temperature profile differences. Figure A5 (left) shows a measure of the vertical resolution of the differently vertically smoothed results. The vertical resolution obtained by the application of AKs is approximated by the full width at half maximum (FWHM) of the AK matrix rows for an example January 2014 global average CrIS AK. The 101 level and ~1 km layer result proxy resolutions are the differences between the pressure levels (done as level below subtracted from current level). The 1 km layer statistics are calculated using approximate fixed-width bins that are ~1 km in the lower atmosphere but increase to ~3 km in the stratosphere. The details of the 1 km layering method can be found in *M. L. Feltz et al.* [2014]. The AK vertical resolution changes from ~220 to 20 hPa between the 300 and 10 hPa levels, whereas the 101 level resolution changes from ~14 to 1 hPa. Due to the logarithmic nature of pressure distribution throughout the height of the atmosphere, while the pressure differences/FWHM decrease with height, the vertical resolution is tending to decrease as well. The 1 km layer results are seen to offer a resolution between that of the 101 level and AK smoothed results. This shows that it is important to use AKs for comparison of stratospheric temperatures.

Figure A5 (right), the NUCAPS minus COSMIC bias and RMS statistics for January 2014 tropics are overlaid for all three types of vertical averaging. The 101 level and ~1 km layer biases look qualitatively similar; however, the ~1 km layer RMS is reduced by ~0.5 K. AK application changes the statistics more than the 1 km layering —the RMS is reduced at all heights and by over 50% in the UTLS, while the large ~1 K magnitude vertical oscillation around 40–100 hPa in the bias is removed. The RMS is seen to grow with increasing height above ~30 hPa, likely due to the ionospheric influence on the top of the RO profile, and grows with decreasing height below the ~300 hPa level due to the water vapor contamination of the RO dry temperature product.

A3. AK Sensitivity Study: Instrument Scan Angle

To estimate the effect of the IR sounder instrument scan angle (which ranges from 0 to 50°) on the AK smoothed temperature difference, example COSMIC and NUCAPS matchup cases from three different latitude zones on 17 February 2016 are investigated. CrIS AKs corresponding to scan angles of 0 and 50° are calculated and applied according to the methodology described above using the NUCAPS temperature and CT carbon dioxide input profiles shown in Figure A6 (first and second panels). Figure A6 (third panel) shows the average sum along the AK row and indicates that the most meaningful AK temperature difference results lie in the ~1–100 hPa region. The effect of the 50° scan angle on the smoothed temperature difference shown in Figure A6 (fourth panel) reveals a potential bias of over ~0.25 K that could be introduced around the 100 hPa region in the tropics and SH polar atmospheres and a bias of over ~0.3 K that could be introduced in the SH polar atmosphere from ~3–9 hPa. To minimize such potential biases, the AK calculation method employed in this paper takes into the account the IR sounder instrument scan angle for each matchup.

Acknowledgments

This work was supported by NOAA/NESDIS grant NA15NES4320001. Flavio Iturbide-Sanchez from NOAA is acknowledged for stimulating discussions on averaging kernel calculations. Thomas August of EUMETSAT is acknowledged for providing the IASI product data used in this study. Thanks are given to the reviewers of this paper who all provided helpful and constructive comments. NASA AIRS products were obtained from the Goddard Earth Sciences Data and Information Services Center (GES DISC) funded by NASA's Science Mission Directorate (SMD). Acknowledgement is given to the NPSO (Taiwan's National Space Organization) and UCAR (University Corporation for Atmospheric Research) for access to the COSMIC data. ARM data were obtained from the Atmospheric Radiation Measurement (ARM) Climate Research Facility, a U.S. Department of Energy Office of Science user facility sponsored by the Office of Biological and Environmental Research. This research was supported by the Office of Biological and Environmental Research of the U.S. Department of Energy as part of the Atmospheric Radiation Measurement (ARM) Climate Research Facility, an Office of Science user facility. Data sources are referenced in section 3.

References

Alexander, P., et al. (2014), Precision estimation in temperature and refractivity profiles retrieved by GPS radio occultations, *J. Geophys. Res. Atmos.*, *119*, 8624–8638, doi:10.1002/2013JD021016.

Anthes, R. A., et al. (2008), The COSMIC/FORMOSAT-3 mission: Early results, *Bull. Am. Meteorol. Soc.*, *89*(3), 313–333.

August, T., et al. (2012), IASI on Metop-A: Operational Level 2 retrievals after five years in orbit, *J. Quant. Spectrosc. Radiat. Transf.*, *113*(11), 1340–1371, doi:10.1016/j.jqsrt.2012.02.028.

Blumstein, D., et al. (2004), IASI instrument: Technical overview and measured performances, optical science and technology, the SPIE 49th Annu. Meeting, Int. Soc. for Opt. and Photonics, doi:10.1117/12.560907.

Boukabara, S. A., et al. (2011), MiRS: An all-weather 1DVAR satellite data assimilation and retrieval system, *IEEE Trans. Geosci. Remote Sens.*, *49*(9), 3249–3272.

Bodeker, G. E., et al. (2016), Reference upper-air observations for climate: From concept to reality, *Bull. Am. Meteorol. Soc.*, *97*(1), 123–135.

Connor, B. J., D. E. Siskind, J. J. Tsou, A. Parrish, and E. E. Remsberg (1994), Ground-based microwave observations of ozone in the upper stratosphere and mesosphere, *J. Geophys. Res.*, *99*, 16,757–16,770, doi:10.1029/94JD01153.

Danzer, J., B. Scherllin-Pirscher, and U. Foelsche (2013), Systematic residual ionospheric errors in radio occultation data and a potential way to minimize them, *Atmos. Meas. Tech.*, *6*(8), 2169–2179, doi:10.5194/amt-6-2169-2013.

Das, U., and C. J. Pan (2014), Validation of FORMOSAT-3/COSMIC level 2 "atmPrf" global temperature data in the stratosphere, *Atmos. Meas. Tech.*, *7*(3), 731–742, doi:10.5194/amt-7-731-2014.

Dee, D. P., et al. (2011), The ERA-Interim reanalysis: Configuration and performance of the data assimilation system, *Q. J. R. Meteorol. Soc.*, *137*(656), 553–597.

Divakarla, M., C. Barnet, M. Goldberg, L. McMillin, E. Maddy, W. Wolf, L. Zhou, and X. Liu (2006), Validation of Atmospheric Infrared Sounder temperature and water vapor retrievals with matched radiosonde measurements and forecasts, *J. Geophys. Res.*, *111*, D09S15, doi:10.1029/2005JD006116.

Divakarla, M., et al. (2009), Validation of AIRS and IASI temperature and water vapor retrievals with global radiosonde measurements and model forecasts, Hyper Spectral Imaging and Sounding of the Environment Topical Meeting, OSA, Vancouver, Canada.

Divakarla, M., et al. (2014), The CrIMSS EDR algorithm: Characterization, optimization, and validation, *J. Geophys. Res. Atmos.*, *119*, 4953–4977, doi:10.1002/2013JD020438.

Feltz, M., R. Knuteson, S. Ackerman, and H. Revercomb (2014), Application of GPS radio occultation to the assessment of temperature profile retrievals from microwave and infrared sounders, *Atmos. Meas. Tech.*, *7*(11), 3751–3762, doi:10.5194/amt-7-3751-2014.

Feltz, M. L., R. O. Knuteson, H. E. Revercomb, and D. C. Tobin (2014), A methodology for the validation of temperature profiles from hyperspectral infrared sounders using GPS radio occultation: Experience with AIRS and COSMIC, *J. Geophys. Res. Atmos.*, *119*, 1680–1691, doi:10.1002/2013JD020853.

Fetzer, E., et al. (2003), AIRS/AMSU/HSB validation, *IEEE Trans. Geosci. Remote Sens.*, *41*(2), 418–443, doi:10.1109/TGRS.2002.808293.

Foelsche, U., et al. (2011), Refractivity and temperature climate records from multiple radio occultation satellites consistent within 0.05%, *Atmos. Meas. Tech.*, *4*(9), 2007–2018, doi:10.5194/amt-4-2007-2011.

Gambacorta, A., et al (2012), The NOAA Unique CrIS/ATMS Processing System (NUCAPS): First light retrieval results, Proceedings of the ITWG meeting, ITWG, Toulouse, France.

Gleason, J. F., Butler, J. J., and Hsu, N. C. (2012, December), The Suomi National Polar-orbiting Partnership Mission: Status and initial results, In AGU Fall Meeting Abstracts (Vol. 1, p. 02).

Goldberg, M. D., H. Kilcoyne, H. Cikanek, and A. Mehta (2013), Joint Polar Satellite System: The United States next generation civilian polar-orbiting environmental satellite system, *J. Geophys. Res. Atmos.*, *118*, 13,463–13,475, doi:10.1002/2013JD020389.

Goldberg, M. D., Y. Qu, L. M. McMillin, W. Wolf, L. Zhou, and M. Divakarla (2003), AIRS near-real-time products and algorithms in support of operational numerical weather prediction, *IEEE Trans. Geosci. Remote Sens.*, *41*(2), 379–389.

Gorbunov, M. E., and G. Kirchengast (2015), Uncertainty propagation through wave optics retrieval of bending angles from GPS radio occultation: Theory and simulation results, *Radio Sci.*, *50*, 1086–1096, doi:10.1002/2015RS005730.
Gorbunov, M. E., et al. (2011), COSMIC radio occultation processing: Cross-center comparison and validation, *J. Atmos. Ocean. Technol.*, *28*(6), 737–751, doi:10.1175/2011JTECHA1489.1.
Hajj, G., et al. (2002), A technical description of atmospheric sounding by GPS occultation, *J. Atmos. Sol. Terr. Phys.*, *64*(4), 451–469.
Han, Y., et al. (2013), Suomi NPP CrIS measurements, sensor data record algorithm, calibration and validation activities, and record data quality, *J. Geophys. Res. Atmos.*, *118*, 12,734–12,748, doi:10.1002/2013JD020344.
He, W., et al. (2009), Assessment of radiosonde temperature measurements in the upper troposphere and lower stratosphere using COSMIC radio occultation data, *Geophys. Res. Lett.*, *36*, L17807, doi:10.1029/2009GL038712.
Ho, S.-P., et al. (2009), Calibration of temperature in the lower stratosphere from microwave measurements using COSMIC radio occultation data: Preliminary results, *Terr. Atmos. Ocean. Sci.*, *20*, 87–100, doi:10.3319/TAO.2007.12.06.01(F3C).
Ho, S.-P., et al. (2012), Reproducibility of GPS radio occultation data for climate monitoring: Profile-to-profile inter-comparison of CHAMP climate records 2002 to 2008 from six data centers, *J. Geophys. Res.*, *117*, D18111, doi:10.1029/2012JD017665.
Ho, S.-P., et al. (2014), Applications of COSMIC radio occultation data from the troposphere to ionosphere and potential impacts of COSMIC-2 data, *Bull. Am. Meteorol. Soc.*, *95*(1), ES18–ES22.
Hoffmann, L., and M. J. Alexander (2009), Retrieval of stratospheric temperatures from Atmospheric Infrared Sounder radiance measurements for gravity wave studies, *J. Geophys. Res.*, *114*, D07105, doi:10.1029/2008JD011241.
Isoz, O., S. A. Buehler, and P. Eriksson (2015), Intercalibration of microwave temperature sounders using radio occultation measurements, *J. Geophys. Res. Atmos.*, *120*, 3758–3773, doi:10.1002/2014JD022699.
Kishore, P., et al. (2016), Evaluating CMIP5 models using GPS radio occultation COSMIC temperature in UTLS region during 2006–2013: Twenty-first century projection and trends, *Clim. Dyn.*, 1–18, doi:10.1007/s00382-016-3024-8.
Klaes, K. D., et al. (2007), An introduction to the EUMETSAT polar system, *Bull. Am. Meteorol. Soc.*, *88*(7), 1085–1096, doi:10.1175/BAMS-88-7-1085.
Kuo, Y.-H., et al. (2005), Comparison of GPS radio occultation soundings with radiosondes, *Geophys. Res. Lett.*, *32*, L05817, doi:10.1029/2004GL021443.
Kursinski, E. R., G. A. Hajj, J. T. Schofield, R. P. Linfield, and K. R. Hardy (1997), Observing Earth's atmosphere with radio occultation measurements using the Global Positioning System, *J. Geophys. Res.*, *102*, 23,429–23,465, doi:10.1029/97JD01569.
Ladstädter, F., et al. (2011), An assessment of differences in lower stratospheric temperature records from (A) MSU, radiosondes, and GPS radio occultation, *Atmos. Meas. Tech.*, *4*(9), 1965–1977, doi:10.1029/2010RS004614.
Ladstädter, F., et al. (2014), Climate intercomparison of GPS radio occultation, RS90/92 radiosondes and GRUAN over 2002 to 2013, *Atmos. Meas. Tech. Discuss.*, *7*, 11,735–11,769, doi:10.5194/amt-8-1819-2015.
Li, Y., et al. (2015), Dynamic statistical optimization of GNSS radio occultation bending angles: An advanced algorithm and its performance analysis, *Atmos. Meas. Tech. Discuss.*, *8*(1), doi:10.5194/amtd-8-811-2015.
Liu, C. L., et al. (2015), Quantifying residual ionospheric errors in GNSS radio occultation bending angles based on ensembles of profiles from end-to-end simulations, *Atmos. Meas. Tech.*, *8*(7), 2999–3019, doi:10.5194/amt-8-2999-2015.
Luo, M., et al. (2007), Comparison of carbon monoxide measurements by TES and MOPITT: Influence of a priori data and instrument characteristics on nadir atmospheric species retrievals, *J. Geophys. Res.*, *112*, D09303, doi:10.1029/2006JD007663.
Mannucci, A., et al. (2006), Generating climate benchmark atmospheric soundings using GPS occultation data, in *Proceedings-SPIE the International Society for Optical Engineering*, vol. 6301, International Society for Optical Engineering, doi:10.1117/12.683973.
Mannucci, A. J., et al. (2011), The impact of large scale ionospheric structure on radio occultation retrievals, *Atmos. Meas. Tech.*, *4*(12), 2837–2850, doi:10.5194/amt-4-2837-2011.
Moncet, J.-L., G. Uymin, A. E. Lipton, and H. E. Snell (2008), Infrared radiance modeling by optimal spectral sampling, *Am. Meteorol. Soc.*, *65*, 3917–3934, doi:10.1175/2008JAS2711.1.
Moncet, J.-L., G. Uymin, P. Liang, and A. Lipton (2015), Fast and accurate radiative transfer in the thermal regime by simultaneous optimal spectral sampling over all channels, *J. Atmos. Sci.*, *72*, 2622–2641, doi:10.1175/JAS-D-14-0190.1.
Murphy, R. E. (2006), The NPOESS preparatory project, in *Earth Science Satellite Remote Sensing*, pp. 182–198 , Springer, Berlin Heidelberg.
Nalli, N. R., et al. (2013), Validation of satellite sounder environmental data records: Application to the Cross-track Infrared Microwave Sounder Suite, *J. Geophys. Res. Atmos.*, *118*, 13,628–13,643, doi:10.1002/2013JD020436.
Nalli, N. R., et al. (2017), Validation of atmospheric profile retrievals from the SNPP NOAA-Unique Combined Atmospheric Processing System: 1. Temperature and moisture, *IEEE Trans.*, 1–11, doi:10.1109/JSTARS.2017.2670504.
Olsen, K. S., et al. (2016), New temperature and pressure retrieval algorithm for high-resolution infrared solar occultation spectroscopy: Analysis and validation against ACE-FTS and COSMIC, *Atmos. Meas. Tech.*, *9*(3), 1063–1082, doi:10.5194/amt-9-1063-2016.
Rodgers, C. D. (1976), Retrieval of atmospheric temperature and composition from remote measurements of thermal radiation, *Rev. Geophys.*, *14*, 609–624, doi:10.1029/RG014i004p00609.
Rodgers, C. D. (1990), Characterization and error analysis of profiles retrieved from remote sounding measurements, *J. Geophys. Res.*, *95*, 5587–5595, doi:10.1029/JD095iD05p05587.
Rodgers, C. D., and B. J. Connor (2003), Intercomparison of remote sounding instruments, *J. Geophys. Res.*, *108*(D3), 4116, doi:10.1029/2002JD002299.
Roman, J., R. Knuteson, T. August, T. Hultberg, S. Ackerman, and H. Revercomb (2016), A global assessment of NASA AIRS v6 and EUMETSAT IASI v6 precipitable water vapor using ground-based GPS SuomiNet stations, *J. Geophys. Res. Atmos.*, *121*, 8925–8948, doi:10.1002/2016JD024806.
Scherllin-Pirscher, B., et al. (2011a), Empirical analysis and modeling of errors of atmospheric profiles from GPS radio occultation, *Atmos. Meas. Tech.*, *4*(9), 1875–1890, doi:10.5194/amt-4-1875-2011.
Scherllin-Pirscher, B., et al. (2011b), Quantifying uncertainty in climatological fields from GPS radio occultation: An empirical-analytical error model, *Atmos. Meas. Tech.*, *4*(9), 2019–2034, doi:10.5194/amt-4-2019-2011.
Schreiner, W., C. Rocken, S. Sokolovskiy, S. Syndergaard, and D. Hunt (2007), Estimates of the precision of GPS radio occultations from the COSMIC/FORMOSAT-3 mission, *Geophys. Res. Lett.*, *34*, L04808, doi:10.1029/2006GL027557.
Steiner, A. K., et al. (2011), GPS radio occultation for climate monitoring and change detection, *Radio Sci.*, *46*, RS0D24, doi10.1029/2010RS004614.
Steiner, A. K., et al. (2013), Quantification of structural uncertainty in climate data records from GPS radio occultation, *Atmos. Chem. Phys.*, *13*(3), 1469–1484, doi:10.5194/acp-13-1469-2013.
Stokes, G. M., and S. E. Schwartz (1994), The Atmospheric Radiation Measurement (ARM) program: Programmatic background and design of the cloud and radiation test bed, *Bull. Am. Meteorol. Soc.*, *75*(7), 1201–1221.

Sun, B., A. Reale, D. J. Seidel, and D. C. Hunt (2010), Comparing radiosonde and COSMIC atmospheric profile data to quantify differences among radiosonde types and the effects of imperfect collocation on comparison statistics, *J. Geophys. Res.*, *115*, D23104, doi:10.1029/2010JD014457.

Sun, B., A. Reale, S. Schroeder, D. J. Seidel, and B. Ballish (2013), Toward improved corrections for radiation-induced biases in radiosonde temperature observations, *J. Geophys. Res. Atmos.*, *118*, 4231–4243, doi:10.1002/jgrd.50369.

Susskind, J., C. D. Barnet, and J. M. Blaisdell (2003), Retrieval of atmospheric and surface parameters from AIRS/AMSU/HSB data in the presence of clouds, *IEEE Trans. Geosci. Remote Sens.*, *41*(2), 390–409, doi:10.1109/TGRS.2002.808236.

Susskind, J., J. M. Blaisdell, L. Iredell, and F. Keita (2011), Improved temperature sounding and quality control methodology using AIRS/AMSU data: The AIRS science team version 5 retrieval algorithm, *IEEE Trans. Geosci. Remote Sens.*, *49*, 883–907, doi:10.1109/TGRS.2010.2070508.

Syndergaard, S. (2000), On the ionosphere calibration in GPS radio occultation measurements, *Radio Sci.*, *35*(3), 865–883, doi:10.1029/1999RS002199.

Tobin, D. C., H. E. Revercomb, R. O. Knuteson, B. M. Lesht, L. L. Strow, S. E. Hannon, W. F. Feltz, L. A. Moy, E. J. Fetzer, and T. S. Cress (2006), Atmospheric Radiation Measurement site atmospheric state best estimates for Atmospheric Infrared Sounder temperature and water vapor retrieval validation, *J. Geophys. Res.*, *111*, D09S14, doi:10.1029/2005JD006103.

Tobin, D., et al. (2013), Suomi-NPP CrIS radiometric calibration uncertainty, *J. Geophys. Res. Atmos.*, *118*, 10,589–10,600, doi:10.1002/jgrd.50809.

Verkhoglyadova, O. P., et al. (2015), Effect of small-scale ionospheric variability on GNSS radio occultation data quality, *J. Geophys. Res. Space Physics*, *120*, 7937–7951, doi:10.1002/2015JA021055.

Wang, K.-N., et al. (2016), Open-loop tracking of rising and setting GPS radio-occultation signals from an airborne platform: Signal model and error analysis, *IEEE Trans. Geosci. Remote Sens.*, *54*(7), 3967–3984, doi:10.1109/TGRS.2016.2532346.

Wee, T.-K., and Y.-H. Kuo (2015), A perspective on the fundamental quality of GPS radio occultation data, *Atmos. Meas. Tech.*, *8*(10), 4281–4294, doi:10.5194/amt-8-4281-2015.

Weng, F., X. Zou, X. Wang, S. Yang, and M. D. Goldberg (2012), Introduction to Suomi national polar-orbiting partnership advanced technology microwave sounder for numerical weather prediction and tropical cyclone applications, *J. Geophys. Res.*, *117*, D19112, doi:10.1029/2012JD018144.

Yunck, T. P., et al. (2009), Use of radio occultation to evaluate atmospheric temperature data from spaceborne infrared sensors, *Terr. Atmos. Ocean. Sci.*, *20*(1), 71–85, doi:10.3319/TAO.2007.12.08.01.

Zeng, Z., et al. (2015), Ionospheric correction of GPS radio occultation data in the troposphere, *Atmos. Meas. Tech.*, *9*(2), 335–346, doi:10.5194/amt-9-335-2016.

Zou, X., et al. (2014), Absolute calibration of ATMS upper level temperature sounding channels using GPS RO observations, *IEEE Trans. Geosci. Remote Sens.*, *52*(2), 1397–1406, doi:10.1109/TGRS.2013.2250981.